Remote Sensing of Environment 112 (2008) 3846–3864

Contents lists available at ScienceDirect

Remote Sensing of Environment

journal homepage: www.elsevier.com/locate/rse

Calibration and validation of hyperspectral indices for the estimation of broadleaved forest leaf chlorophyll content, leaf mass per area, leaf area index and leaf canopy biomass

Guerric le Maire [a,b,*], Christophe François [a], Kamel Soudani [a], Daniel Berveiller [a], Jean-Yves Pontailler [a], Nathalie Bréda [c], Hélène Genet [c], Hendrik Davi [d], Eric Dufrêne [a]

[a] Laboratoire Ecologie Systématique et Evolution, UMR CNRS - Univ Paris Sud - AgroParisTech, 91405 Orsay, France
[b] CIRAD, UR 80 Fonctionnement et pilotage des écosystèmes de plantations, Montpellier, F-34398, France
[c] Ecologie et Ecophysiologie Forestières, UMR INRA-UHP 54820 Champenoux, France
[d] Ecologie des Forêts Méditerranéennes, UR 629, INRA, 84914 Avignon, France

ARTICLE INFO

Article history:
Received 12 October 2007
Received in revised form 6 June 2008
Accepted 6 June 2008

Keywords:
Chlorophyll
LMA
SLA
Leaf biomass
EO1 Hyperion
ASD Fieldspec
LAI
PROSPECT
SAIL
PROSAIL

ABSTRACT

This article aims at finding efficient hyperspectral indices for the estimation of forest sun leaf chlorophyll content (CHL, µg cm^{-2}_{leaf}), sun leaf mass per area (LMA, $g_{dry\ matter}\ m^{-2}_{leaf}$), canopy leaf area index (LAI, $m^2_{leaf}\ m^{-2}_{soil}$) and leaf canopy biomass (B_{leaf}, $g_{dry\ matter}\ m^{-2}_{soil}$). These parameters are useful inputs for forest ecosystem simulations at landscape scale. The method is based on the determination of the best vegetation indices (index form and wavelengths) using the radiative transfer model PROSAIL (formed by the newly-calibrated leaf reflectance model PROSPECT coupled with the multi-layer version of the canopy radiative transfer model SAIL). The results are tested on experimental measurements at both leaf and canopy scales. At the leaf scale, it is possible to estimate CHL with high precision using a two wavelength vegetation index after a simulation based calibration. At the leaf scale, the LMA is more difficult to estimate with indices. At the canopy scale, efficient indices were determined on a generic simulated database to estimate CHL, LMA, LAI and Bleaf in a general way. These indices were then applied to two Hyperion images (50 plots) on the Fontainebleau and Fougères forests and portable spectroradiometer measurements. They showed good results with an RMSE of 8.2 µg cm^{-2} for CHL, 9.1 g m^{-2} for LMA, 1.7 m^2 m^{-2} for LAI and 50.6 g m^{-2} for Bleaf. However, at the canopy scale, even if the wavelengths of the calibrated indices were accurately determined with the simulated database, the regressions between the indices and the biophysical characteristics still had to be calibrated on measurements. At the canopy scale, the best indices were: for leaf chlorophyll content: $ND_{chl}=(\rho_{925}-\rho_{710})/(\rho_{925}+\rho_{710})$, for leaf mass per area: $ND_{LMA}=(\rho_{2260}-\rho_{1490})/(\rho_{2260}+\rho_{1490})$, for leaf area index: $D_{LAI}=\rho_{1725}-\rho_{970}$, and for canopy leaf biomass: $ND_{Bleaf}=(\rho_{2160}-\rho_{1540})/(\rho_{2160}+\rho_{1540})$.

1. Introduction

Forest ecosystems are well-studied at the stand scale. However, in order to better understand their functioning and response to environmental changes, it is necessary to up-scale this knowledge to the scale of the entire forest or small region (Landsberg, 2003; Makela et al., 2000). One way to reach this objective is to use ecosystem models that are validated with local-scale observations and applied to larger areas. For a large scale simulation, a selection of spatially-parameterized input parameters is necessary. The selection of the main spatial parameters should meet the following criteria (le Maire et al., 2005):

(i) to be a parameter to whish the model is sensitive,
(ii) to be spatially variable at the scale of interest (for instance between stands), and to have a larger variability at this scale than at finer scale (e.g., inter-stand vs. intra-stand variability),
(ii) to have a non-linear model response: this strengthens the need for spatialization of the parameter if the simulation results are averaged.

A study with a particular forest process-based ecosystem model has shown that a number of parameters are sensitive in this model (Dufrêne et al., 2005). Many of these parameters are spatially variable between stands, some of them having a non-linear response (Davi

* Corresponding author. Laboratoire Ecologie Systématique et Evolution, UMR CNRS - Univ Paris Sud - AgroParisTech, 91405 Orsay, France.
E-mail address: guerric.le_maire@cirad.fr (G. le Maire).

0034-4257/$ – see front matter © 2008 Elsevier Inc. All rights reserved.
doi:10.1016/j.rse.2008.06.005

et al., 2006). Among these parameters, in addition to soil parameters driving the soil water budget, the following vegetation parameters were identified:

- leaf nitrogen content (N_{leaf}), which is directly involved in the photosynthesis calculation. Experimental measurements have shown that this parameter is highly correlated with leaf chlorophyll content (CHL, µg cm^{-2}) for sun leaves (see Section 4.7),
- annual maximum leaf mass per area (LMA) of sun leaves (leaves of the canopy that are not shadowed by other leaves), a parameter that enables conversion of leaf area to leaf biomass (B_{leaf}), which is used in many processes in the model,
- annual maximum leaf area index (LAI), which drives many processes like radiation interception, canopy photosynthesis and litter amount.

The objective of the present study is to assess the possibility of estimating essential parameters of forest ecosystem models (LMA, LAI, CHL and B_{leaf}) using hyperspectral satellite images on large areas, and to estimate the obtained accuracy.

The use of indices on hyperspectral images has two major advantages. First, the most informative wavelengths of the 400–2500 nm region can be selected. Second, it allows the use of a narrow spectrum feature necessary for assessing vegetation biochemical properties (Broge & Mortensen, 2002). Many studies have shown that hyperspectral measurements can be used to quantify biophysical characteristics of the vegetation at leaf scale (Gitelson et al., 2003; le Maire et al., 2004; Zhao et al., 2005) or at canopy scale using in situ data, airborne sensors like AVIRIS, CASI and HyMap, or spaceborne sensors like Hyperion and CHRIS.

Different methods exist to retrieve canopy characteristics from reflectance measurements (Blackburn, 2007; Kimes et al., 2000; Weiss & Baret, 1999):

(i) *Indices and/or multiple regressions*: the principle is to combine several reflectances measured on narrow or large spectral bands into mathematical combinations and to correlate them to a particular characteristic of the observed surface. These relationships are calibrated based on an experimental or simulated reflectance database (built up on radiative transfer models). These methods are simple, but have some limits: when calibrated to an experimental database, the representativeness of the relationships is limited to the representativeness of the database. Moreover, indices and multiple regressions may be sensitive to more than one single characteristic. They are also sensitive to atmospheric conditions, view geometry, and spatial resolution, and therefore they must usually be calibrated for each image.

(ii) *Model inversions*: this method uses models that simulate reflectance spectra from canopy and soil characteristics. As noted by Bacour et al. (2006), inversion techniques based on pre-computed reflectance database are often preferred to more computationally heavy iterative methods for operational applications. Among the computationally efficient methods often used are Look-Up Tables (e.g. Knyazikhin et al., 1998) and Neural Networks (e.g. Bacour et al., 2006; Baret et al., 2007). Both methods are dependent on the simulated training database. Inversion of such models often gives a large number of different possible solutions. Moreover, uncertainties in measurements and models may result in large variation in results (Combal et al., 2003).

The best way to find efficient indices would be to use a large measurement database, with many images and canopy conditions. Such a large database with hundreds of measurements is feasible at the leaf scale but is not conceivable at the forest scale. Moreover, indices calibrated on a particular forest canopy database could be unsuitable in other forests.

This issue leads us to create a large synthetic database containing reflectance spectra and their corresponding canopy characteristics. Such a database has many advantages: many canopy characteristics are represented (thousands of spectra); the influence of each characteristic can be totally decoupled from that of others; and the effect of a particular characteristic on the spectra is based on physical processes that are modeled at a small scale. Therefore, well established indices obtained on such a large simulated database may potentially be applied to a wide range of spectra. However, the use of a model relies on its capacity to correctly simulate the reflectance of a wide range of canopies. Thus, it is essential to test these indices on experimental measurements. The representativeness of the simulated database is therefore critical.

In this study, we generate two simulated databases, one at leaf scale with the PROSPECT model, and one at canopy scale coupling the PROSPECT leaf model with the SAIL canopy radiative transfer model (PROSAIL). At leaf scale, we continue the study done in le Maire et al. (2004) using an improved and newly calibrated version of the PROSPECT model (Feret et al., 2008), and a larger experimental database. The work at this scale is a first step to interpret the results at the canopy scale and explain possible discrepancies. At canopy scale, we use a multi-layer version of the SAIL model (Weiss et al., 2001), which is able to represent the vertical LMA profile. The study is restricted to canopies with LAI greater than 3 to correspond with the big-leaf representation of SAIL. These simulated databases are used to find best indices of CHL and LMA at leaf scale, and CHL, LMA, LAI and B_{leaf} at canopy scale.

Results are tested against measurements at both scales. At leaf scale we used a large database of 246 spectra and 49 species. At canopy scales, experimental measurements consist of ground measurements on small and mature canopies with a portable spectroradiometer, and hyperspectral images for two distinct forests measured with the Hyperion satellite.

We first describe the PROSPECT and SAIL models, simulated databases and the determination method of best spectral indices. Then, we present the experimental protocols for the measurements (leaf reflectance measurements, in situ measurements and satellite remote sensing data). The results are given at leaf and canopy scale for the determination of CHL, LMA, LAI and leaf biomass.

2. Model description, simulated databases and best indices determination method

2.1. The Leaf reflectance model PROSPECT

An improved (1-nm resolution) and recalibrated version of the leaf reflectance model PROSPECT has been used in this study (Feret et al., 2008). The PROSPECT model (Jacquemoud & Baret, 1990; Jacquemoud et al., 1996) considers the leaf as a succession of absorbing layers. The new version calculates the leaf hemispherical reflectance and transmittance between 400 and 2500 nm with a 1-nm step as a function of leaf structure index (N_{struc}), leaf chlorophyll content (CHL, µg/cm^2), leaf water content (Cw, g/cm^2), and leaf mass area (LMA, g/m^2).

2.2. Multi-layer PROSAIL model description

The SAIL radiative tranfer model is a turbid medium model. It describes the canopy as horizontally homogeneous, where leaves absorb, reflect, and transmit radiation (Verhoef, 1984). This model has been validated by many studies on numerous vegetation types (e.g. Andrieu et al., 1997; Goel & Thomson, 1984; Major et al., 1992). The radiative transfer equation is solved using an *n*-flux approximation. The radiation is considered as four fluxes: diffuse, direct, upward and downward (Kubelka & Munk, 1931; Suits, 1972). The system is described as four differential equations for the four fluxes. The solar

Table 1
Parameters used to build the 6006 spectra of the PROSPECT database, and the 149,688 spectra of the PROSAIL database (other parameters are nadir observation, solar zenithal angle=θ, satellite/sun angle=90°, diffuse radiation=80%, average leaf angle=27°)

	Values		
	Minimum	Step	Maximum
PROSPECT database input variables			
CHL (μg/cm^2)	10	10	110
LMA (g/m^2)	20	10	140
Cw (cm)	0.004	0.004	0.024
Nstruc	1.1	0.2	2.3
PROSAIL database input variables			
CHL (μg/cm^2)	10	10	110
LMA (g/m^2)	20	20	140
Cw (cm)	0.004	0.004	0.024
Nstruc	1.1	0.4	2.3
LAI (m^2/m^2)	3	0.7	8.6
θ (°)	30	15	60
p_{soil}	0	0.5	1

radiation is divided into diffuse and direct, and their proportions change with total radiation. The leaf inclination distribution function is ellipsoidal (Campbell, 1986). The model does not represent canopy horizontal heterogeneity (due to fractional vegetation cover, soil variability, understory and shadowing), which can be critical for low LAI; thus, we restricted the present study to stands of LAI greater than 3. With this restriction, we consider the SAIL model a good compromise among realism, computational speed, and the number of input parameters for the present study, despite the complexity of the studied system.

Coupling of PROSPECT and SAIL has been performed many times (Weiss et al., 2001). PROSPECT simulates the reflectance and transmittance of individual leaves, properties that are required as input into SAIL. The basic version of SAIL represents the canopy as vertically homogeneous. This assumption is not true in the forest canopy, which has vertical gradients of biophysical features (notably a gradient in LMA, see Appendix A) that are likely to influence the overall canopy reflectance. For this reason, the one-layer SAIL model was transformed into a multi-layer SAIL model, with *n* layers (typically 50) corresponding to *n* stacked one-layer SAIL models (Weiss et al., 2001). Appendix A describes the multi-layer PROSAIL model parameterization.

2.3. Simulated databases

Two simulated databases have been created, one with leaf reflectances (PROSPECT) and one with canopy reflectances (PROSAIL). These databases are generated using a range of input parameters, and the reflectances are computed for every combination of these parameters (Table 1). To ensure generalizable results, a uniform distribution was chosen for each varied parameter, so that a reflectance spectrum obtained with extreme parameter values has the same weight as other spectra on the indices' calibration procedure. Some parameters are considered constant (see Table 1 legend).

In order to reproduce in the simulations the observed radiometric noise of real measured reflectances, a random noise has been added to each spectrum of both databases (leaf and canopy). This step is important to eliminate noise sensitive indices and indices with artificially close wavelengths (le Maire et al., 2004). An additive random Gaussian noise with a standard deviation of 3% of reflectance amplitude has been applied on each wavelength of each reflectance spectrum of the PROSPECT and PROSAIL database.

2.4. Determination of best indices

Seven types of indices have been used in this study, ranging from very simple (R) to more sophisticated (DDn) (see Table 4 in the result section). These types of indices were obtained from a literature review (le Maire et al., 2004). The new DDn index, based on the DD index described in le Maire et al. (2004), shares with the DD index the same underlying principle based on the double-peak of derivatives near the red-edge, but the formulation is simpler:

$$DDn = 2 \times \rho_{\lambda} - \rho_{\lambda-\Delta} - \rho_{\lambda+\Delta}$$

with λ wavelength in the red-edge and Δ distance in nanometers. This index, based on the red-edge properties, cannot be used on leaves with very low chlorophyll content (<10 μg cm^{-2}), where the red-edge features are less visible.

A process flow diagram is given in Fig. 1 to show the methodology adopted in this study. The determination of indices is composed of two steps: (1) determination of the best wavelength for a given type of index, and (2) determination of the index vs. parameter regression curve. A search of indices was done for CHL and LMA at leaf and canopy level using the PROSPECT and PROSAIL databases, and for LAI and B_{leaf} at canopy scale using the PROSAIL database.

The calibration is performed by testing all possible combinations of wavelength for an index type, with wavelengths varying by 5 nm. For each combination, index values are calculated for each spectra of the database. A second order polynomial is fit between index values and the characteristic to be predicted (CHL, LMA, LAI or B_{leaf}). Higher order polynomials were tested and did not result in significant improvement.

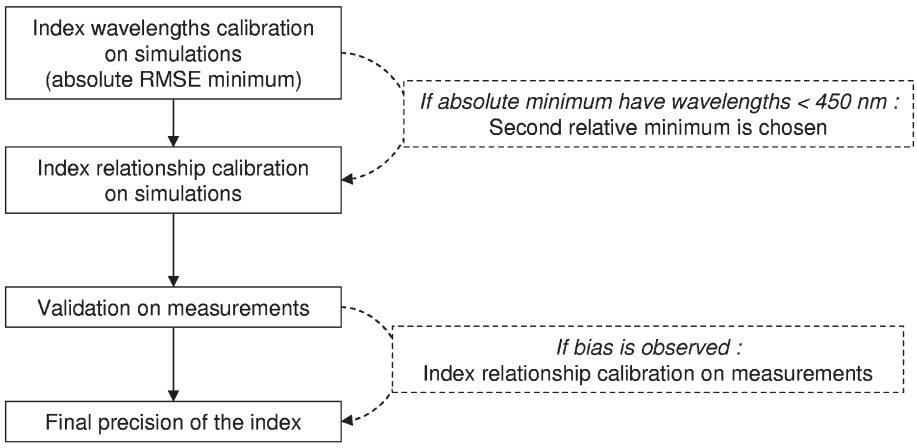

Fig. 1. Process flow diagram explaining the study scheme. The dashed line represents adaptations made to the normal process.

The root mean square error (RMSE) is commonly used to compare different indices and is also used in this study.

$$\mathrm{RMSE} = \sqrt{\frac{\sum_{i=1}^{n} (P_i - o_i)^2}{n}}$$

with P_i the predicted value, O_i the observation for the ith spectrum, and n the number of spectra.

For a given type of index, the best combination of wavelengths has the lowest RMSE.

2.5. Matrix representation of RMSE

A 2-D graphical representation of RMSE has been constructed for indices using two reflectances in two wavelengths ($\rho_{\lambda 1}$ and $\rho_{\lambda 2}$). The RMSE calculated for each index is represented as a two dimensional contour plot with axes λ_1 and λ_2. This representation as a matrix contour plot has several advantages. The absolute minimum can be directly seen, and the extent of the local minimum area can be easily evaluated. In addition, all local low RMSE zones are visible, with their respective RMSE values. Other studies have used such representations, using the r-squared of the fitted relationship instead of the RMSE (Hansen & Schjoerring, 2003). The RMSE is more useful for our purpose because it shows the precision of the index directly, and it is the best statistic to evaluate the error associated with the model.

3. Experimental protocols

3.1. Reflectance measurements at leaf scale

Spectra were measured for *Acer pseudoplatanus* (n=248) and other temperate species (n=48) that were cultivated in a large range of fertility, radiation and watering conditions to obtain a large range of leaf chlorophyll, leaf dry matter and leaf water content. Reflectance and transmittance were measured with the FieldSpec-FR spectroradiometer (Analytical Spectral Devices, Boulder, Colorado-USA) coupled with an integrative sphere (Li-Cor 1800, Li-COR, Inc., Lincoln, Nebraska, USA). Measurements of chlorophyll, LMA and water content are detailed in Feret et al. (2008). Hereafter, this database is called the ANGERS database.

3.2. Ground based reflectance measurements at canopy scale

3.2.1. Study sites, LAI, CHL and LMA measurements

Ground based measurements were performed on three distinct canopies: one small canopy of seedlings and two young forest canopies.

The small canopy is a 4 m^2 tree plantation of 180 seedlings of three-year-old *Fagus sylvatica* (beech). Young trees were about 40 cm height in 2002. A thin layer of mould was added to homogenise the soil surface. The small canopy is homogeneous in height, density, and incident solar radiation, and has a LAI similar to what is observed for an adult stand. In addition to this small canopy, some pot seedlings were used for extra measurements.

Reflectance measurements have been done from small scaffolding built to the north of the small canopy to avoid shadowing. This allows easy changes to the measurement height and location.

Four different protocols were used for the small canopy, in order to maximize the variability of LAI, CHL and LMA. These methods are presented in Appendix B. Leaf nitrogen content was also measured for some plots. Table 2 presents the number of reflectance spectra measured, and the corresponding mean and range of CHL, LMA and LAI.

Reflectance and associated biophysical measurements were also conducted for large canopies in Hesse forest, France (48°40′N, 7°05′E, 300 m) in 2002. This forest is composed of 90% beech. Two stands of this forest were studied: the first one (HESSE1) is a natural regeneration of beech, age 37 years in 2002, the second one (HESSE2) is a 10-year-old smaller regeneration with different species (*Fagus sylvatica*, *Quercus petraea*, *Quercus robur*, *Carpinus betulus*). Average tree heights are 17.5 m for HESSE1 and 5 m for HESSE2. Scaffoldings on both sites allowed measurement of reflectance from 2 m above the canopy and sampling of leaves for biochemical analysis. In HESSE1, the canopy reflectance was also measured from a 30 meter tower. LAI was estimated at both sites with a Licor LAI-2000 (LI-COR Inc., Nebraska, USA). CHL was measured on sun leaves with a Chlorophyll Meter SPAD-502 (Minolta Camera, Osaka, Japan). The leaves used for these measurements were kept cold, and their LMA was obtained following the method described in Appendix B. A total of 14 spectra have been measured at Hesse sites (Table 2).

3.2.2. Canopy reflectance estimates with the FieldSpec spectroradiometer

All measurements were performed on clear days, with a vertical angle of view and with the sun around local noon. The portable spectroradiometer FieldSpec-FR was used to measure the spectral reflectance of the canopies described above. This instrument measures radiance through an optical fiber between 350 and 2500 nm. The spectral resolution is 3 nm in the visible and 10 nm in the near and middle infrared. A 25 cm square panel covered by Spectralon (Labsphere Inc., Sutton, NH, USA) material was used for the reference measurements. This material is almost Lambertian and gives very high reflectance between 350 and 2500 nm. The reflectance of an object is the ratio of the reflected light to the incident radiance. The incident radiance coming from the sun is measured with the Fieldspec directed towards the Spectralon at a distance of about 10 cm. During

Table 2
Mean values of chlorophyll content (CHL, μg cm^{-2}), leaf mass per area (LMA, g m^{-2}) and leaf area index (LAI, m^2 m^{-2}) measured for the different experiments. Standard deviations and minimum/maximum values are given (std and min–max)

Scale	Experiment	n reflec.	Instrument	CHL			LMA			LAI		
		Spectrum		Mean	Min	Max	Mean	Min	Max	Mean	Min	Max
Leaf	ANGERS	246	FieldSpec+sphere	35.2	0.8	107	51.4	16.5	157.2	n.a.	n.a.	n.a.
Small canopy	Seasonal	14	FieldSpec	18.7	13.2	26.3	49.9	31.4	67.5	5.7	3.5	8.0
Small canopy	Spatial	4	FieldSpec	21.8	20.3	23.8	68.1	66.1	72.6	8.3	8.3	8.3
Small canopy	Potted tree spacing	3	FieldSpec	23.7	23.6	23.8	56.9	56.8	57.0	4.3	3.4	5.1
Small canopy	Defoliation	23	FieldSpec	30.5	28.2	30.9	56.7	51.4	61.3	6.3	3.21	8.3
Forest canopy	Hesse	14	FieldSpec	45.7	25.2	67.1	90.4	74.5	108.2	7.4	5.0	9.3
Forest	Fontainebleau	14	Hyperion	55.7	31.5	81.2	116.2	91.5	134.6	5.3	3.7	7.1
Forest	Fougères	33 (28 for LAI)	Hyperion	38.9	33.8	46.8	89.9	76.9	101.1	5.6	3.3	7.7
Leaf	PROSPECT	6006	Simulations	60	10	110	80	20	140	n.a.	n.a.	n.a.
Canopy	PROSAIL	149,688	Simulations	60	10	110	80	20	140	5	1	9

Values prescribed for simulated databases are given for comparison.

Table 3
Characteristics of the two Hyperion satellite images: date and time of acquisition, view and sun geometry

Site	Acquisition date	Time UT	Sun elevation (°)	Sun azimuth (°)	Look angle (°)
Fontainebleau	04 Sept 2004	1030	46.50	151.9	3.57
Fougères	06 Aug 2006	1045	53.85	143.6	1.95

all measurements the Fieldspec sensor is fixed above the canopy, and the Spectralon is alternately placed under the sensor for the reference measurement or shifted away when the sensor is measuring the canopy. To take into account error measurements and small variations in incident light that occur even on a clear day, the alternation between reference and object radiance measurement was repeated at least 25 times. The object radiance was divided by the mean of reference radiances measured before and after. The quality of the 25 reflectance spectra obtained was visually checked, and spectra that had high residuals were eliminated. Most of the time less than five spectra were eliminated, and the remaining spectra were very similar. The average of the remaining spectra was calculated and used for the study as a single spectrum. Since measurements were conducted during clear days, the signal to noise ratio is high because the solar radiance intensity is high and temporal variations are low. Three regions of the spectrum are noisy because of high absorption of

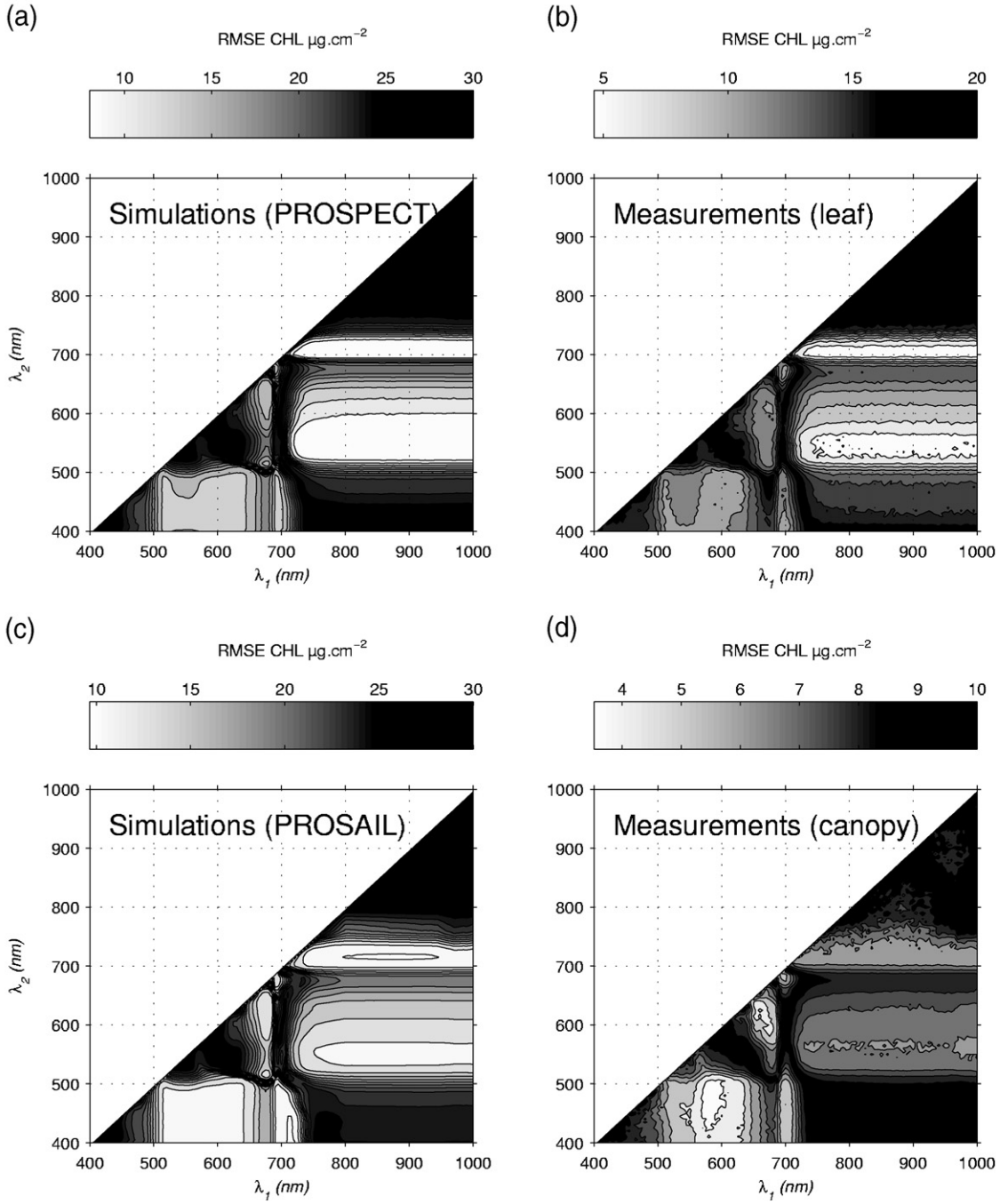

Fig. 2. Matrices representing the RMSE of leaf chlorophyll content (CHL) prediction with ND type indices ($ND=(\rho_{\lambda 1}-\rho_{\lambda 2})/(\rho_{\lambda 1}+\rho_{\lambda 2})$). Calculations are performed on simulations and the measurements database at leaf and canopy scale. The leaf database used is the ANGERS database, the canopy database is obtained with ASD measurements (see Table 2). At both the leaf and canopy scales the RMSE with leaf chlorophyll content is represented. Value scales are not the same between plots.

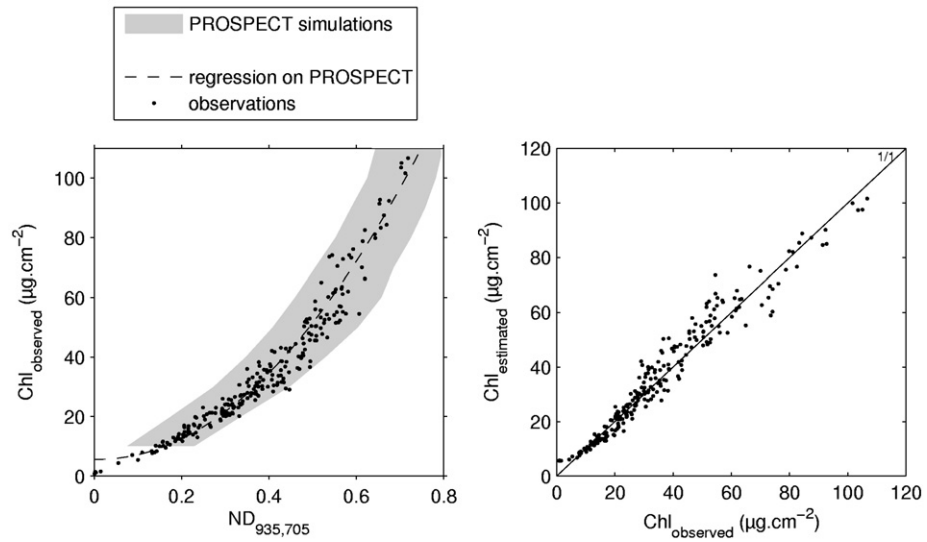

Fig. 3. Best leaf-scale chlorophyll index calibrated to simulations ($ND_{935,705}$) and tested on ANGERS observations. Grey area covers the results for the 6006 PROSPECT simulated reflectance. The dashed line is the second order polynomial fit to simulation results and is used for the calculation of $CHL_{estimated}$ (right). Black dots are the results for ANGERS measurements.

atmospheric water vapor (1360–1400 nm, 1820–1940 nm and 2200–2500 nm). Note that in this study, an assumption is made that moderate sun and/or view angles result in relatively small radiative effects, and that neglecting soil/understory background reflectance anisotropy is acceptable when working with data from nadir-viewing instruments and closed canopies (for ground or satellite measurements presented hereafter).

3.3. Canopy reflectance estimates with Hyperion

3.3.1. Study sites, LAI, CHL and LMA measurements

Two deciduous forest sites were chosen for satellite remote sensing acquisition.

The first site is the Fontainebleau forest, located southeast of Paris (48°25′N, 2°40′E, mean altitude 120 m). It is a large forest of over 17,000 ha in a region characterized by a temperate climate, with a mean annual temperature of 10.6 °C and mean precipitation of 750 mm fairly well distributed throughout the year. This forest is composed of oaks (*Quercus robur*, *Quercus petraea*), scots pines (*Pinus sylvestris*) and beech. Only 10% of the forest is mixed.

The second site is the Fougères Forest, located in the west of France (48°23′N, 1°10′O, mean altitude of 150 m). It is a smaller forest extending over 1660 ha in a region characterized by an oceanic climate (mean temperature 11.2 °C, mean precipitation 900 mm fairly well distributed throughout the year). This forest is more homogeneous than the Fontainebleau forest in terms of soil types and species (it is dominated by beech).

These forests are actively managed by the French National Forest Office ("Office National des Forêts", ONF), and divided into management units localized on a GIS database (with the software ArcGIS 8.1, Environmental Systems Research Institute Inc., Redlands, California). These management units, called "stands" in this study, are of similar age and homogeneous in species, stand structure, and tree density. The parts of the forests studied in this work have flat topography.

For the Fontainebleau forest, a total of 17 beech and oak stands were selected. Measurements were carried out in early July 2003 for all stands and in early September 2004, two days after Hyperion image acquisition. For the seven stands not measured in 2004, LMA and CHL were determined using a robust relationship established using 2003 and 2004 measurements (R^2 = 0.85).

Table 4
Leaf level indices: results of the general types of indices calibrated to the PROSPECT simulated database for the CHL and LMA

Index type	Formulation	λ_1 (nm)	λ_2 (nm)	λ_3 (nm)	Regression calibrated on PROSPECT	$RMSE_{PROSPECT}$	$RMSE_{observations}$
CHL indices, leaf level					CHL (µg cm^{-2}) =	(µg cm^{-2})	(µg cm^{-2})
R	$\rho_{\lambda1}$	705			$1101.6R^2 - 783.5R + 147.7$	13.18	7.54
D	$\rho_{\lambda1} - \rho_{\lambda2}$	980	720		$1161.7D^2 - 129.7D + 4.2$	10.96	8.73
SR	$\rho_{\lambda2}/\rho_{\lambda1}$	970	710		$212.8SR^2 - 383.9SR + 181.3$	7.10	4.93
ND	$(\rho_{\lambda1} - \rho_{\lambda2})/(\rho_{\lambda1} + \rho_{\lambda2})$	935	705		$199.2ND^2 - 13.6ND + 7.16$	7.16	4.65
mND	$(\rho_{\lambda1} - \rho_{\lambda2})/(\rho_{\lambda1} + \rho_{\lambda2} - 2\rho_{\lambda3})$	935	715	405	$141.7mND^2 + 98.5mND + 0.5$	9.25	4.80
mSR	$(\rho_{\lambda1} - \rho_{\lambda3})/(\rho_{\lambda2} - \rho_{\lambda3})$	970	715	405	$179.3mSR^2 - 3.1mSR + 6.1$	8.46	4.87
DDn	$2*\rho_{\lambda1} - \rho_{(\lambda1-\lambda2)} - \rho_{(\lambda1+\lambda2)}$	710	50		$392.8DDn^2 - 171.8DDn + 24.7$	6.53*	8.36*
LMA indices, leaf level					LMA (g m^{-2}) =	(g m^{-2})	(g m^{-2})
R	$\rho_{\lambda1}$	2300			$526.9\ R^2 - 510.6R + 129.4$	31.9	28.0
D	$\rho_{\lambda1} - \rho_{\lambda2}$	2395	2295		$(5.6D^2 - 2.1D + 0.2) * 10^3$	25.2	29.8
SR	$\rho_{\lambda1}/\rho_{\lambda2}$	2295	1500		$-48.6SR^2 + 276.9SR - 259.0$	16.1	24.4
ND	$(\rho_{\lambda1} - \rho_{\lambda2})/(\rho_{\lambda1} + \rho_{\lambda2})$	2295	1500		$734.9ND^2 + 358.7ND - 34.1$	15.9	24.2
mND	$(\rho_{\lambda1} - \rho_{\lambda2})/(\rho_{\lambda1} + \rho_{\lambda2} - 2\rho_{\lambda3})$	2285	1335	2400	$237.2mND^2 + 53.9mND - 91.0$	19.2	26.3
mSR	$(\rho_{\lambda1} - \rho_{\lambda3})/(\rho_{\lambda2} - \rho_{\lambda3})$	2265	1620	2400	$-1.3mSR^2 - 51.7mSR - 66.9$	21.2	28.3
ND	$(\rho_{\lambda1} - \rho_{\lambda2})/(\rho_{\lambda1} + \rho_{\lambda2})$	*1710*	*1340*		(see legend)		*16.4*

Best wavelengths were found for the PROSPECT database. $RMSE_{PROSPECT}$ and $RMSE_{observations}$ values are obtained with the second-order fit to PROSPECT. The last line in italics corresponds to an index using a local minimum for the wavelengths, and fit to observations: $LMA = 1986.2ND^2 + 401.6ND - 15.3$.
*Used on leaves with CHL > 10 µg cm^{-2}.

For the Fougères forest, 33 beech stands were chosen. Measurements were carried out in June 2006. The same measurement protocols were used in Fontainebleau and Fougères. Within each stand, 5 to 15 representative trees were selected for CHL and LMA measurements (on sun leaves). The LAI-2000 was used for ground LAI measurements.

Details of the measurements for CHL, LMA and LAI are given in Appendix C.

In order to test the validity of the stand as a measurement object, analysis of variance (ANOVA) tests were performed on CHL and LMA measurements to detect if CHL and LMA were actually statistically variable among stands. The 5 to 15 trees per stand were used as a group of values for which the intra-group and inter-group variance were calculated and compared. Results show that there is a stand effect in Fougères and Fontainebleau for CHL and LMA ($p<0.05$). This reinforces the choice of the stand as studied object, and the need to obtain stand-scale estimations of CHL and LMA for inputs to ecosystem models.

3.3.2. Hyperion image acquisition and processing

The Hyperion imaging spectrometer onboard the NASA Earth Observing-1 spacecraft is a push broom sensor that provides 242 spectral bands at 10 nm intervals over the 400–2500 nm region. The spatial resolution is 30 m, and an image is 7.7 km wide and 42 km long.

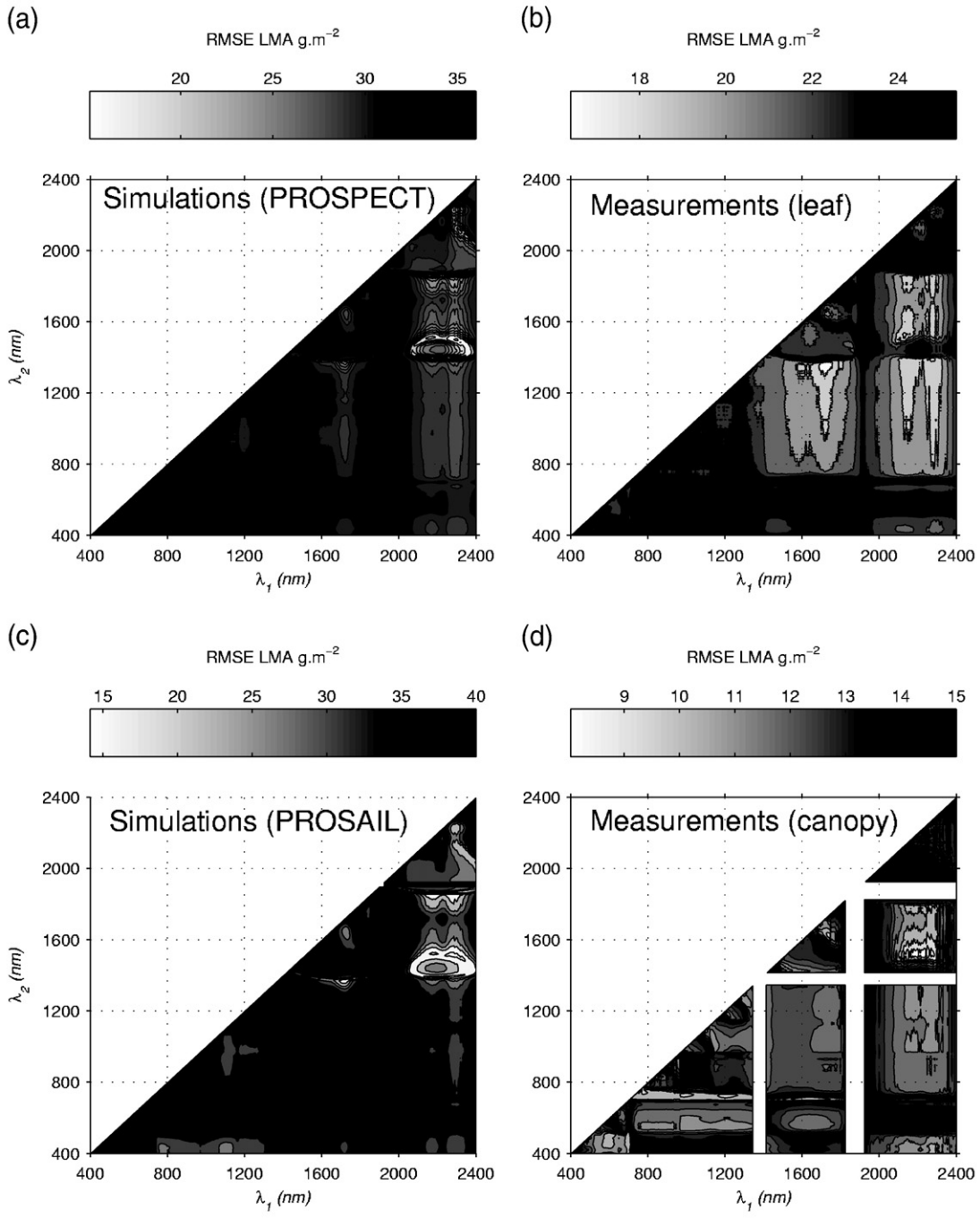

Fig. 4. Matrices representing the RMSE of leaf mass per area (LMA) prediction with ND type indices ($ND=(\rho_{\lambda1}-\rho_{\lambda2})/(\rho_{\lambda1}+\rho_{\lambda2})$). Calculations are conducted on simulations and the measurements database at leaf and canopy scale. The leaf database used is the ANGERS database, the canopy database is obtained with ASD measurements (see Table 2). At both the leaf and canopy scales the RMSE with leaf mass per area is represented. Value scales are not the same between plots.

Some of the bands are not calibrated and thus not usable. Other bands are not used in this study because of very low signal to noise ratio due to atmospheric absorption. Here, 165 bands out of the 242 have been used (bands 8–57, 80–120, 130–163, 185–224).

Two images were acquired: one above Fontainebleau forest and one above Fougères (see specification on Table 3). These images are cloud free above the forest, but the Fougères image shows some clouds around it. A series of processing steps were necessary to obtain the final reflectance of the stands (Appendix D).

For both sites, polygons were drawn to select the sampled portion of the stands. A 30 meter buffer was applied to avoid edge effects. The reflectance spectra of selected pixels were extracted and averaged to obtain an average reflectance for each stand. The use of the reflectance is therefore based on spatially coherent objects, and this has been shown to be an efficient way to obtain meaningful estimations of canopy biophysical variables (Atzberger, 2004).

4. Results

4.1. Leaf scale CHL indices

The ND type index, which is a normalized difference of two wavelengths, is calibrated on the PROSPECT simulated reflectance database. Fig. 2a shows the RMSE represented as contour plots. All local minima have RMSE values better than 10 μg cm^{-2}. The size of these areas gives visual information on the necessary spectral precision. The plot is shown between 400 and 1000 nm because no significant additional information is found after 1000 nm for CHL.

A contour plot is obtained in the same way for the measurement database (Fig. 2b.). The two contour plots (a) and (b) are very similar in terms of RMSE values and patterns. These similarities give confidence in the model's ability to simulate the behavior of a ND type index in relation to CHL for a wide range of wavelengths.

From PROSPECT simulations, the best index is $ND_{935,705}$, with a RMSE of 7.16 μg cm^{-2}. Fig. 2a shows that the important wavelength of this index is λ_2 = 705 nm, whereas the other wavelength can be ranged between 750 and 1000 nm without affecting much the predictive strength of the index. Another zone of minimum RMSE is the zone with $\lambda_2 \in$[550–600 nm] and $\lambda_1 \in$[750–1000 nm]. This area is larger, which means that these indices do not require very narrow and precise spectral bands.

Fig. 3a shows the relationship between CHL and the $ND_{935,705}$ index for simulated and measured reflectances. This index is efficient because it meets the three following conditions: (i) the area of the simulation results shows no saturation and a narrow dispersion of predictions, (ii) the measurements are well-aligned, and (iii) there is a very good match between simulations and measurements, with only few points outside the boundaries of the simulated database and no bias (Fig. 3b).

Fig. 3b shows the relationship between measurements and predictions using a second order polynomial fit calibrated from PROSPECT simulations (see Table 4). The RMSE of the estimation of measurements is 4.65 μg cm^{-2}.

Other types of indices have also been tested and are reported in Table 4. For each type of index, the one giving the best RMSE for the simulated database is reported in Table 4 with its wavelength(s), its regression equation and its RMSE for the simulated database. Finally, the validation RMSE is calculated for the experimental database ANGERS and also given in the Table 4 ($RMSE_{observations}$). The results show that ND is the best index for the simulated database.

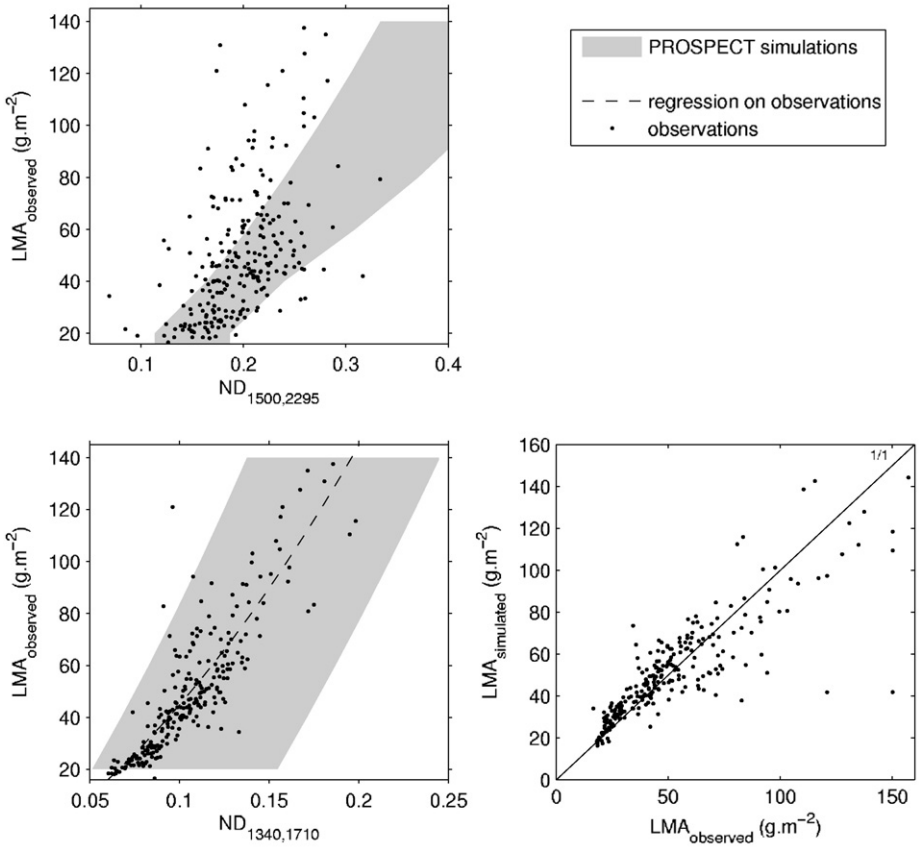

Fig. 5. Best leaf-scale LMA index calibrated to simulations ($ND_{1500,2295}$) and tested on ANGERS observations (top). For comparison, the best LMA index calibrated to observation ($ND_{1340,1710}$) results are also presented (bottom).

4.2. Leaf scale LMA indices

Table 4 shows that the ND type index is the most recommended index for leaf LMA prediction for calibration and validation with respect to RMSE. There is no improvement when using more sophisticated indices like mND and mSR types.

RMSE matrices for LMA estimated from PROSPECT simulations and measurements are represented in Fig. 4 for ND indices. The spectral range is increased because most of the dry matter signal is in the near and middle infrared. The order of magnitude of the RMSE for the PROSPECT database is higher than for CHL: the RMSE simulated is about 25% of the LMA values, whereas it is about 15% for CHL. The comparison with the matrix obtained for measurements shows similarities in the regions of low RMSE, but discrepancies in their relative values. In fact, the main minimum area in simulations (λ_1 = 2100 to 2300 nm and λ_2 around 1500) is not the main minimum area in the RMSE matrix of measurements (Fig. 4a; Table 4). Fig. 5a shows the plot of the best ND index calibrated to simulations ($ND_{2295,1500}$) against LMA: the simulation points cover quite a large area, which means that the best index found for simulations has a high associated error. The measurements are very scattered, and some of the points fall outside the boundaries of the simulations. Even if the relationship is significant between the index and ND, the use of this index for LMA estimations would lead to high error.

For comparison purposes, the best index found on the experimental database $ND_{1710,1340}$ was plotted (Fig. 5b and c). This figure shows that even the best index calibrated to the experimental database shows high scattering: the RMSE is 16.4 g m^{-2} in this case. This means that the LMA is a much more difficult leaf characteristic to capture with reflectance indices.

4.3. Canopy scale CHL indices

At canopy scale, the PROSAIL database is used to find the best indices. SR and ND types of indices give slightly lower RMSE values than other types of indices (Table 5). The general pattern of the matrix representation of ND type of indices is similar to that obtained at the leaf level, except that the absolute level of RMSE is higher (Fig. 2c). At canopy level, the area with $\lambda_2 \in$[400–500 nm] and λ_1 ~ 710 nm and the area with λ_2 ~ 710 nm and $\lambda_1 \in$[750–1000 nm] are the most efficient ones for simulations.

Interestingly, the location of the RMSE minima areas are similar to the coefficient of correlation map obtained by Hansen and Schjoerring (2003) for chlorophyll density on wheat. Comparison of the RMSE matrix obtained from our small canopy scale measurements with those from a portable spectroradiometer also reveals many similarities in areas of minimum RMSE. It confirms the ability of the PROSAIL model to simulate well the link between ND spectral index and canopy leaf chlorophyll content.

The absolute minimum of simulations is located at wavelengths 710 and 400 nm. This particular index gives good results at the small canopy scale (FieldSpec measurements) (Fig. 2d). However, this index

Table 5
Canopy level indices: results of the 7 general types of indices calibrated to PROSAIL simulated database for the four characteristics

Index type	Formulation	λ_1 (nm)	λ_2 (nm)	λ_3 (nm)	$RMSE_{PROSAIL}$	$RMSE_{observations}$
CHL indices, canopy level					(µg cm^{-2})	(µg cm^{-2})
R	$\rho_{\lambda1}$	710			10.03	n.s.
D	$\rho_{\lambda1}-\rho_{\lambda2}$	705	505		9.98	n.s.
SR	$\rho_{\lambda2}/\rho_{\lambda1}$	710	400		9.92	n.s.
ND	$(\rho_{\lambda1}-\rho_{\lambda2})/(\rho_{\lambda1}+\rho_{\lambda2})$	710	400		9.84	n.s.
mND	$(\rho_{\lambda1}-\rho_{\lambda2})/(\rho_{\lambda1}+\rho_{\lambda2}-2\rho_{\lambda3})$	715	860	455	9.94	n.s.
mSR	$(\rho_{\lambda1}-\rho_{\lambda3})/(\rho_{\lambda2}-\rho_{\lambda3})$	720	860	450	9.98	n.s.
DDn	$2*\rho_{\lambda1}-\rho_{(\lambda1-\lambda2)}-\rho_{(\lambda1+\lambda2)}$	730	50		9.95*	n.s.
ND	*$(\rho_{\lambda1}-\rho_{\lambda2})/(\rho_{\lambda1}+\rho_{\lambda2})$*	*710*	*925*		*n.s.*	*8.24*
LMA indices, canopy level					(g m^{-2})	(g m^{-2})
R	$\rho_{\lambda1}$	1100			21.89	n.s.
D	$\rho_{\lambda1}-\rho_{\lambda2}$	2380	2300		18.35	n.s.
SR	$\rho_{\lambda2}/\rho_{\lambda1}$	2280	1395		14.55	n.s.
ND	$(\rho_{\lambda1}-\rho_{\lambda2})/(\rho_{\lambda1}+\rho_{\lambda2})$	2280	1395		14.14	n.s.
mND	$(\rho_{\lambda1}-\rho_{\lambda2})/(\rho_{\lambda1}+\rho_{\lambda2}-2\rho_{\lambda3})$	2275	1920	1520	14.91	n.s.
mSR	$(\rho_{\lambda1}-\rho_{\lambda3})/(\rho_{\lambda2}-\rho_{\lambda3})$	2275	1920	1520	14.54	n.s.
ND	*$(\rho_{\lambda1}-\rho_{\lambda2})/(\rho_{\lambda1}+\rho_{\lambda2})$*	*2260*	*1490*		*n.s.*	*9.15*
LAI indices					(m^{-2} m^{-2})	(m^{-2} m^{-2})
R	$\rho_{\lambda1}$	925			1.55	n.s.
D	$\rho_{\lambda1}-\rho_{\lambda2}$	1725	970		1.31	1.71
SR	$\rho_{\lambda2}/\rho_{\lambda1}$	925	400		1.62	n.s.
ND	$(\rho_{\lambda1}-\rho_{\lambda2})/(\rho_{\lambda1}+\rho_{\lambda2})$	925	400		1.62	n.s.
mND	$(\rho_{\lambda1}-\rho_{\lambda2})/(\rho_{\lambda1}+\rho_{\lambda2}-2\rho_{\lambda3})$	1195	2220	915	1.69	n.s.
mSR	$(\rho_{\lambda1}-\rho_{\lambda3})/(\rho_{\lambda2}-\rho_{\lambda3})$	1195	2220	915	1.69	n.s.
NDVI	$(\rho_{\lambda1}-\rho_{\lambda2})/(\rho_{\lambda1}+\rho_{\lambda2})$	800	680		1.78	n.s.
B_{leaf} indices					(g m^{-2})	(g m^{-2})
R	$\rho_{\lambda1}$	1100			117.9	n.s.
D	$\rho_{\lambda1}-\rho_{\lambda2}$	1720	1470		93.2	n.s.
SR	$\rho_{\lambda2}/\rho_{\lambda1}$	2245	1395		75.4	n.s.
ND	$(\rho_{\lambda1}-\rho_{\lambda2})/(\rho_{\lambda1}+\rho_{\lambda2})$	2190	1390		75.1	n.s.
mND	$(\rho_{\lambda1}-\rho_{\lambda2})/(\rho_{\lambda1}+\rho_{\lambda2}-2\rho_{\lambda3})$	1375	2400	2265	79.2	n.s.
mSR	$(\rho_{\lambda1}-\rho_{\lambda3})/(\rho_{\lambda2}-\rho_{\lambda3})$	1380	2400	2190	77.4	n.s.
ND	*$(\rho_{\lambda1}-\rho_{\lambda2})/(\rho_{\lambda1}+\rho_{\lambda2})$*	*2160*	*1540*		*n.s.*	*50.6*

Best wavelengths are found for the PROSAIL database. Results in italics represent the minimum for another local minimum area. "n.s." are not significant results, meaning that indices and the relationship between the index and the characteristic leads to insignificant results when applied to observations. $RMSE_{observations}$ values are obtained with following second-order fits on observations: $CHL = 162.8ND^2 - 41.8ND + 6.8$; $LMA = -134.4ND^2 + 350.0ND + 33.1$; $LAI = 70.8D^2 + 38.2D - 8.0$; $B_{leaf} = 250.5ND^2 + 1269.4ND - 82.1$.
*Used on leaves with CHL > 10 µg cm^{-2}.

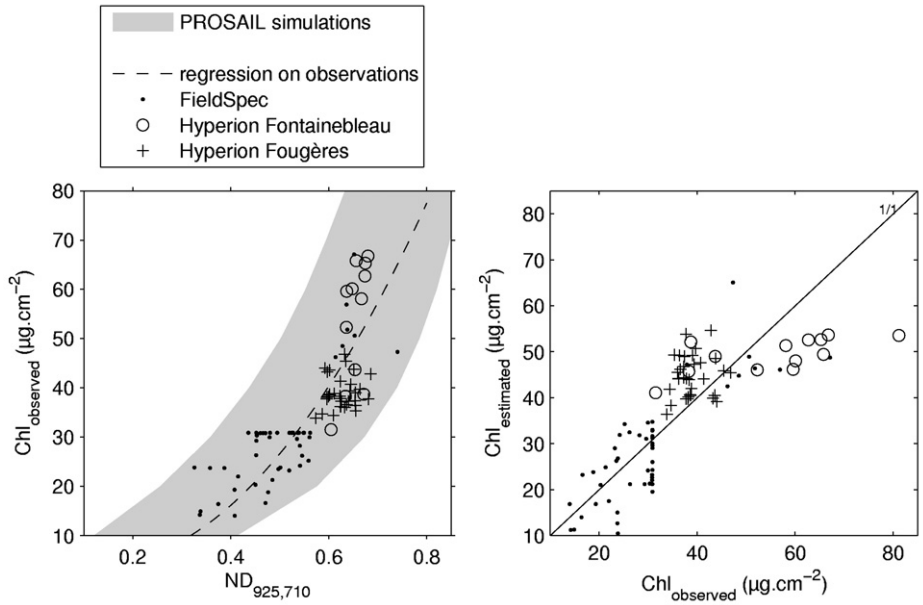

Fig. 6. Best canopy-scale chlorophyll index calibrated to simulations ($ND_{925,710}$) and tested on small canopy and Hyperion observations. Grey area covers the results for the PROSAIL 149688 simulated reflectance. The dashed line is the second order polynomial fit to observations and is used for the calculation of $CHL_{estimated}$ (right).

cannot be used with Hyperion data because most of the bands below 450 nm have too low signal-to-noise ratios. Instead we focused on the $\lambda_1 \in$[720–1000 nm] and λ_2~710 nm region, which is the second minimum of the simulations (Fig. 2c). We choose the local minimum at 925 nm and 710 nm for the simulation database (in the same minimum area, Hansen and Schjoerring obtained 732 nm and 717 nm on their experimental database).

Fig. 6a shows that the λ_1=925 nm and λ_2=710 nm index gives fair results for simulations, the width of the simulation point zone being larger than at leaf scale, but the relationship has low saturation. When adding data from the different experiments (FieldSpec measurements, Hyperion at Fougères and Fontainebleau), most of the points are within the boundaries of the simulations. There is a good match between the points from ground measurements and those from Hyperion reflectances. The points measured in the tall forest at Hesse fell within the same range of chlorophyll content and index values than the points measured with Hyperion. Considering only Hyperion data, the regression between $ND_{925,710}$ and CHL is significant ($p<0.05$) for the Fontainebleau forest but not significant for the Fougères forest. This is mainly due to the range of CHL values that is higher in Fontainebleau than in Fougères (Table 2). Contrary to simulation results, a saturation appears with measurements when the $ND_{925,710}$ value is greater than 0.65. This leads to an underestimation of CHL for values of CHL greater than 50 µg cm^{-2}.

When using a regression between the index and CHL calibrated to the simulation database, the CHL is predicted with a RMSE of 8.86 µg cm^{-2}. If the regression is calibrated to measurements, the RMSE is slightly reduced to 8.25 µg cm^{-2} (Table 5).

The $ND_{925,710}$ index was found to be significantly correlated to leaf chlorophyll content in earlier studies (Hansen and Schjoerring, 2003; Zarco-Tejada et al., 2004b; Zarco-Tejada et al., 2001), with the 925 nm wavelength being sometimes 800 or 750 nm (same minimum area in Fig. 2). The wavelength near 710 nm, in the red-edge zone, is essential in this index (Fig. 2).

4.4. Canopy scale LMA indices

The RMSE matrix calculated for the PROSAIL simulations for ND type of indices is very similar to that obtained at the leaf scale with

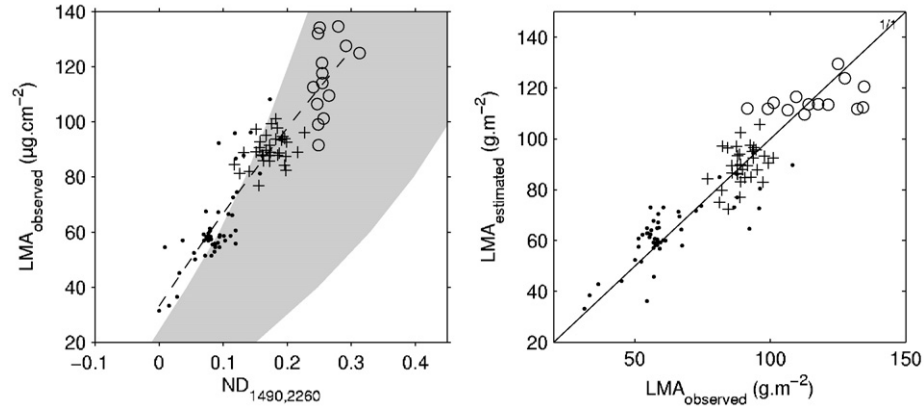

Fig. 7. Best canopy-scale LMA index calibrated to simulations ($ND_{1490,2260}$) and tested on small canopy and Hyperion observations. See Fig. 6 for the legend.

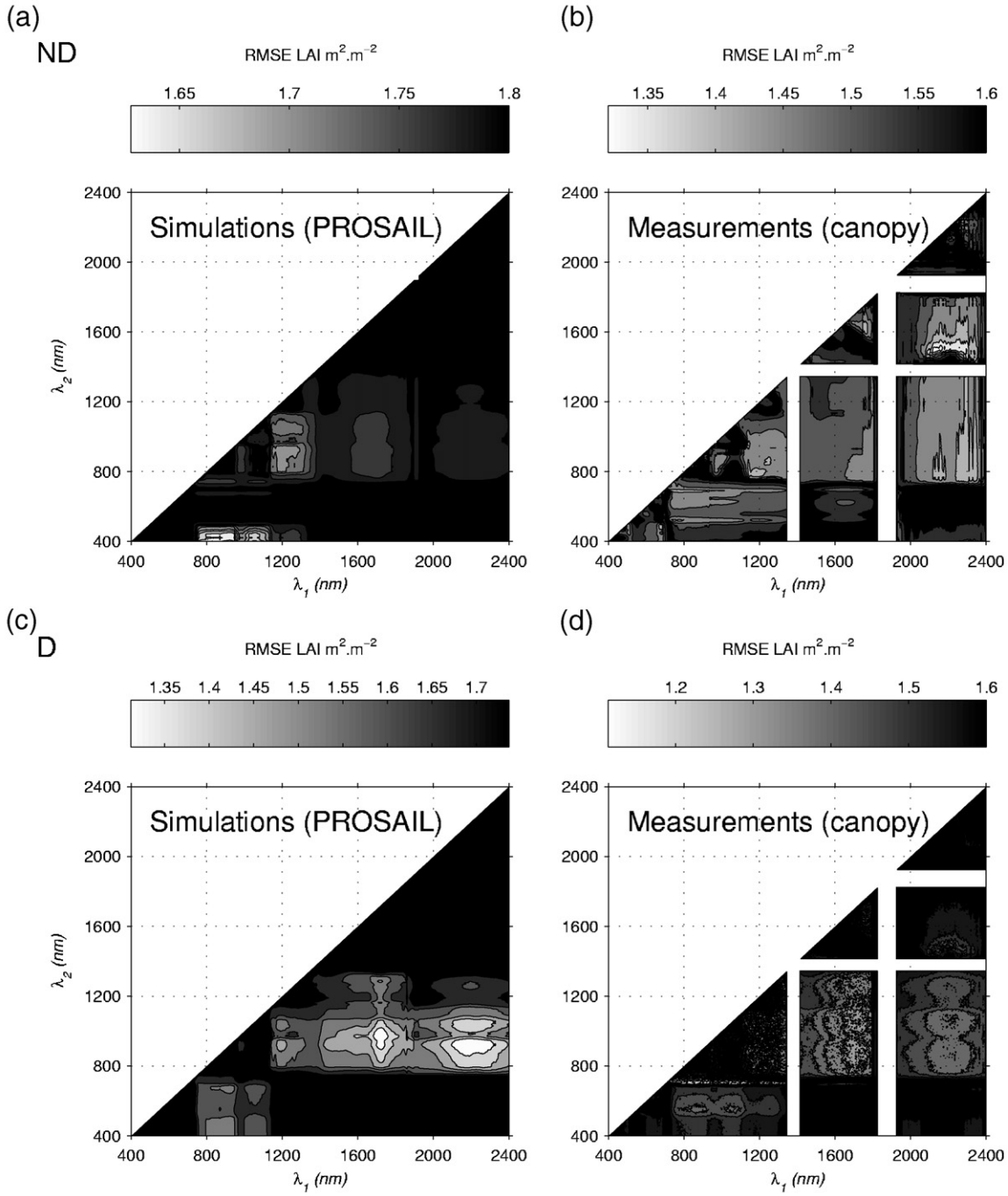

Fig. 8. Matrices representing the RMSE of leaf area index (LAI) prediction with ND type indices (ND=($\rho_{\lambda1}-\rho_{\lambda2}$)/($\rho_{\lambda1}+\rho_{\lambda2}$)) (a and b) and D type indices (D=($\rho_{\lambda1}-\rho_{\lambda2}$)) (c and d). Calculations are done on simulations and the measurements database at canopy scale. The canopy database is obtained with ASD measurements (see Table 2). The RMSE with leaf area index is represented. Value scales are not the same between plots.

PROSPECT simulations (Fig. 4a and c). The matrix obtained at the small canopy scale (Fig. 4d) has the same pattern as that calculated from leaf scale measurements for λ_1 and λ_2 above 1400 nm. Some similarities are found between the simulation and measurement matrices, with the λ_2 ~1500 and $\lambda_1 \in$[2100–2300 nm] region appearing in both contour plots.

The absolute minimum is obtained with the index $ND_{2280,1395}$ (Table 5). However, this index belongs to a very small minimum area, which means that the 1395 nm wavelength is absolutely necessary. This wavelength is in a spectral region of high water vapor absorbance by atmosphere, and is therefore not suitable for measurements under natural atmospheric conditions. As a consequence, the second minimum area was chosen with the index $ND_{2260,1490}$.

Fig. 7 shows that the relationship between the PROSAIL-based $ND_{2260,1490}$ index and the canopy LMA is very scattered. This index gives fair results when applied to measurements. First of all, most of the measurements are within or close to the boundaries of the simulations. They are well aligned between small scale measurements and measurements with Hyperion. However, if solely Hyperion measurements are used for a particular forest, the relationship is only significant for Fougères. We can see from simulations that this index is less efficient for high LMA, which can explain part of the poor results obtained for Fontainebleau, which has higher LMA values (Table 2).

When the regression on simulations is directly used, the RMSE of the LMA estimation from the $ND_{2260,1490}$ index is unacceptable (35.3 g m^{-2}), with a general tendency to underestimate the LMA by

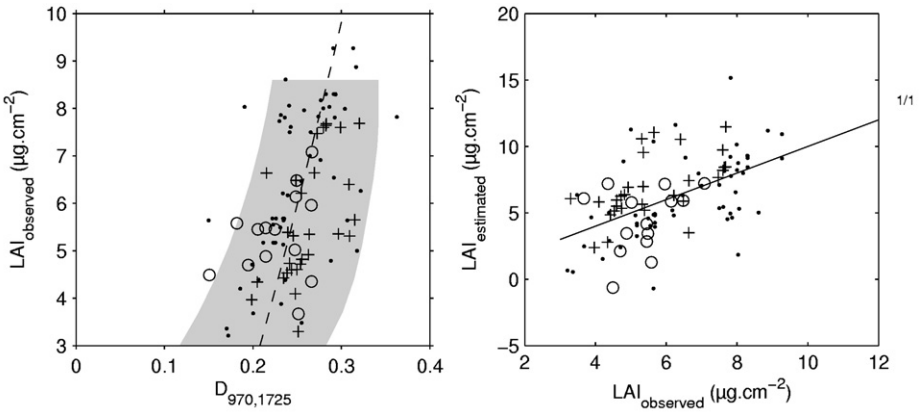

Fig. 9. Best LAI index calibrated to simulations ($D_{970,1725}$) and tested on small canopy and Hyperion observations. See Fig. 6 for the legend.

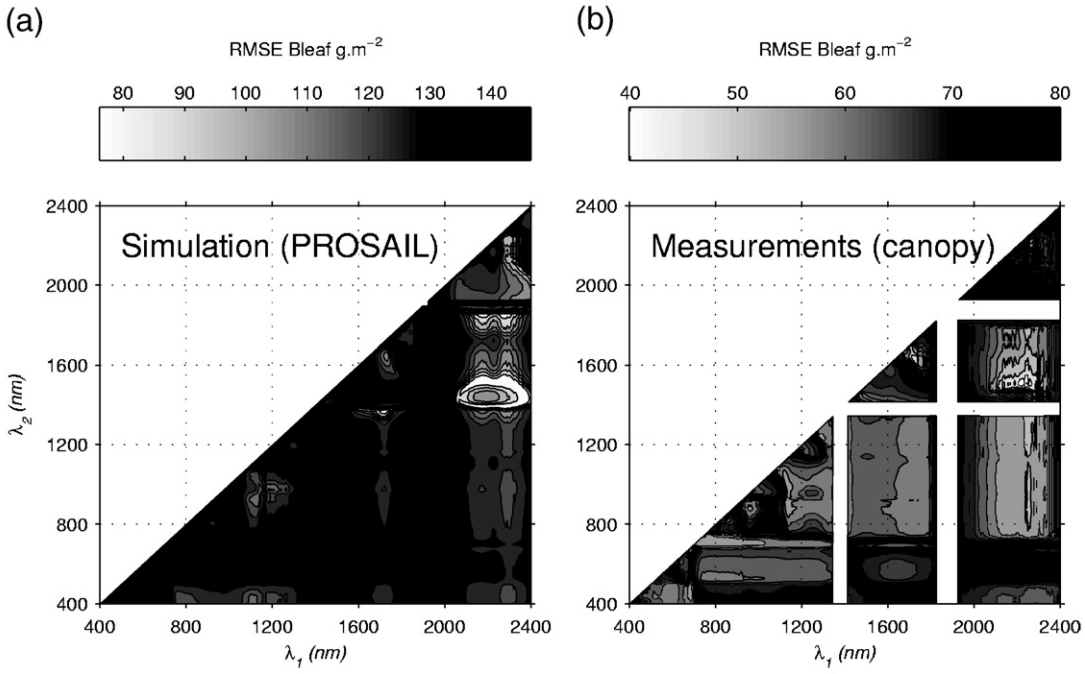

Fig. 10. Matrices representing the RMSE of total leaf dry biomass (B_{leaf}) prediction with ND type indices ($ND=(\rho_{\lambda 1}-\rho_{\lambda 2})/(\rho_{\lambda 1}+\rho_{\lambda 2})$). Calculations are performed on simulations and the measurements database at canopy scale. The canopy database is obtained with ASD measurements (see Table 2). The RMSE with leaf biomass is represented. Value scales are not the same between plots.

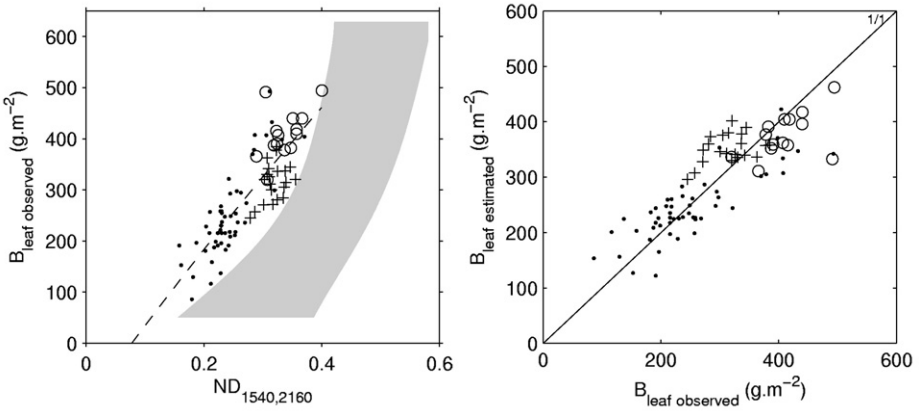

Fig. 11. Best B_{leaf} index calibrated to simulations ($ND_{1540,2160}$) and tested on small canopy and Hyperion observations. See Fig. 6 for the legend.

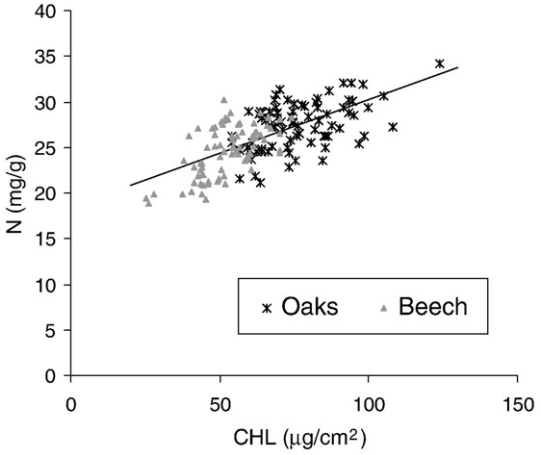

Fig. 12. Nitrogen content (N, mg/g) as a function of CHL (µg/cm^2) for sun leaves of Oak and Beech measured at the Fontainebleau forest (N=0.1185CHL+18.42; r^2=0.66; p<0.001).

about 20 g m^{-2}. When using the regression based on measurements, the RMSE of the $ND_{2260,1490}$ index becomes 9.15 g m^{-2} (Table 5), which is much more satisfactory.

4.5. Canopy scale LAI indices

For LAI estimation (with LAI greater than 3 in this study), the best index found is of D type, which is a simple difference between two wavelengths (Table 5). This is a surprising result, since most of the time ND type indices are used, especially the NDVI (=$ND_{800,680}$). RMSE matrices are calculated for these two types of indices for both simulations and measurements (Fig. 8). We find that ND types have a minimum zone with $\lambda_2 \in$[400 500 nm] and $\lambda_1 \in$[780 1000 nm] (RMSE=1.62 m^2 m^{-2}, Table 5). The NDVI zone (i.e. $ND_{800,680}$) does not appear as efficient for the simulation database (RMSE=1.78 m^2 m^{-2}, Table 5). Comparison between PROSAIL simulations and measurement matrices show many discrepancies, meaning that PROSAIL does not represent well the relationship of the ND index with LAI.

This matrix remains unchanged if we use a third order polynomial or a (−1/ln(ND)) transformation instead of a second order polynomial to fit the ND vs. LAI relationship. For the D type of index, RMSE matrices from PROSAIL simulations and from measurements show a similar pattern. The RMSE range for the D type of index is also better than the ND type for measurements (best indices 1.62 m^2 m^{-2} for ND type, 1.31 m^2 m^{-2} for D type).

The best index found for simulations is the index $D_{1725,970}$, which does not use reflectance in the visible. This index gives reasonable results: there is a good match between simulations and measurements, and measurements are well aligned between FieldSpec and the two Hyperion images (Fig. 9). Regression between the indices and LAI is significant (p<0.05) for both the Fougères and Fieldspec measurements, but not for the Fontainebleau forest. The regression could be fit either to simulations or to measurements, and gives similar RMSE values (1.71 m^2 m^{-2} when fitted to simulations). These results show that prediction for high values of LAI remains a problem with this type of index because of its saturation for LAI greater than 3–4. This is a well-known problem with the index-based prediction of LAI, as shown in previous studies (Anderson et al., 2004; Birky, 2001; Fassnacht et al., 1997; Qi et al., 2000; Soudani et al., 2006; Wang et al., 2005). It can be overcome in this type of ecosystem using other information like spatial variability (le Maire et al., 2006).

4.6. Canopy scale B_{leaf} indices

Leaf biomass is calculated as the product of the LMA profile and LAI. Table 5 shows the best indices for B_{leaf} estimation found for the PROSAIL database. The best indices found are the ND, SR, mND, and mSR types. However, like LMA indices, they have one of their wavelengths in an atmospheric water vapor high absorption band, and therefore cannot be tested against measurements. When discarding water absorption areas, $ND_{1540,2160}$ becomes the best index for B_{leaf} estimation. Fig. 10 shows that the RMSE matrix of B_{leaf} is a combination of the LMA and LAI matrices (Figs. 4 and 8), with LMA characteristics highly visible in the $ND_{1500,2200}$ region. Comparison with the measurements matrix shows many discrepancies, mainly from differences between these measured and simulated LAI ND matrices (Fig. 8a and b).

Results for the $ND_{1540,2160}$ index are shown in Fig. 11. There is a high bias between simulations and measurements. Indices simulated by PROSAIL are too high. When fit to measurements, regression between the $ND_{1540,2160}$ index and Bleaf is significant at the Fontainebleau site with p<0.05, and p=0.07 at Fougères site, with a global RMSE of 50.6 g m^{-2}.

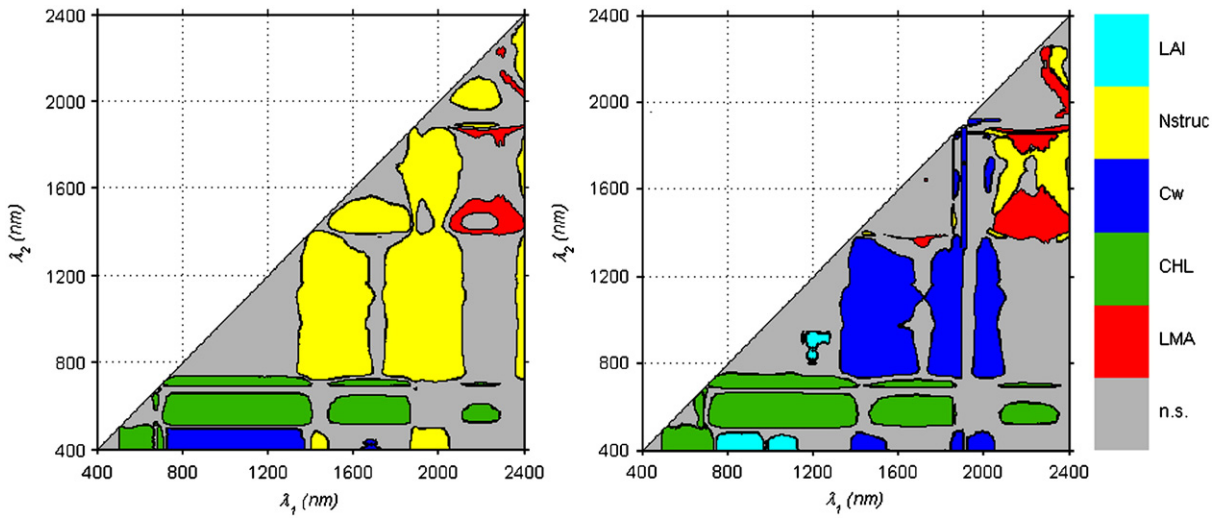

Fig. 13. Representation of lower RMSE zones for ND indices (ND=($\rho_{\lambda1}-\rho_{\lambda2}$)/($\rho_{\lambda1}+\rho_{\lambda2}$)) for leaf-scale PROSPECT simulations (left) and canopy-scale PROSAIL simulations (right). Nstruc is PROSPECT leaf structure parameter, Cw is leaf water content. Non-significant indices zones (n.s.) give high RMSE for all five parameters.

4.7. Nitrogen determination

Although CHL is a physiological indicator of stand health conditions, which can potentially justify its direct use, CHL estimations cannot be directly used as input parameters in forest ecosystem models (contrary to LMA, LAI and B_{leaf}). Instead, photosynthesis models use nitrogen concentration by leaf area for each LAI layer of the canopy. The nitrogen content of sun leaves (N_m, in mg g^{-1} of leaf dry matter) is linked to the CHL content by unit area (μg cm^{-2}) (Fig. 12 and (Filella et al., 1995; Moran et al., 2000; Yoder and Pettigrew-Crosby, 1995)) and is approximately constant from the top to the bottom of canopy (Appendix A, Fig. A1). To retrieve the nitrogen content per leaf area (N_a, in g m^{-2}) profile from hyperspectral data, one can follow the following steps using the results given in this study:

1- estimate the LAI using the $D_{1725,970}$ index or another method
2- estimate the sun leaves LMA using the $ND_{2260,1490}$ index
3- calculate the LMA profile using total LAI found in step 1 and the extinction coefficient with the equation in Appendix A
4- estimate the sun leaves CHL using the $ND_{710,925}$ index
5- estimate the sun leaves N_m from CHL values (Fig. 12)
6- estimate the N_a profile using LMA profile and assuming a constant value of leaf N_m.

This method is associated with a number of errors resulting from estimation uncertainties and hypotheses about vertical profiles. This method gives slightly better results than the direct correlation between nitrogen and the reflectance spectrum mainly because there is a greater signal from the chlorophyll content on the spectral reflectance. The RMSE for estimating sun leaves N_m is 2.7 mg g^{-1} for the direct method and 2.3 mg g^{-1} for the CHL-based method (results are based on the 18 cases where nitrogen measurements were available). This gives an error of 13.6% of the mean, a value near that obtained by Coops et al. (2003) and Smith et al. (2003) with Hyperion data. Another advantage is the use of simulated reflectance, which is possible with the chlorophyll method.

5. General discussion

Results at canopy scale varied from good (CHL and LMA) to fair (LAI and B_{leaf}) with the wavelengths determined on the synthetic database. However, the regression between indices and biophysical characteristics had to be calibrated to measurements. The error observed with simulation-based regressions may be due either to errors in the PROSAIL model, to a bias in the simulated database inputs, or both.

The PROSPECT sub-model of PROSAIL was shown to perform well at leaf scale, except for LMA retrieval: the sun-leaf LMA at canopy level was obtained with an overall error of 11 g m^{-2}, although it was 16.4 g m^{-2} on leaf level for the best indices. This result is surprising because up-scaling generally increases errors and noise. This may be due to the fact that at leaf scale the experimental database was created to have a very large range of variability in species and growth conditions. In contrast, measurements on forests show less variability (Table 2).

More generally, measurements at canopy scale may not be extensive enough to represent the simulation database range, or the simulation database may be too broad compared to measurements, which may create a bias. Table 2 shows that the range of LMA, CHL and LAI used for simulations are similar to measured values, but this may not be the case for other SAIL inputs like leaf angle.

Concerning the models, the PROSPECT sub-model of PROSAIL was shown to perform well at leaf scale. The PROSAIL model has proven efficient in the findingof indices (see RMSE matrices). However, it is possible that the relatively simple SAIL model does not accurately simulate the absolute value of the reflectance of a tree canopy because canopies are never perfectly homogeneous, even with a LAI greater than 3 (as considered in this study). Zarco-Tejada et al. (2001) have shown that for closed canopies of deciduous stands with LAI greater than 3, there was practically no shadow effect when pigment-sensitive indices, rather than entire canopy reflectance spectra, are simulated with models and compared to observed above-canopy reflectances. For LAI<3, some particular effects of clumping and shadows are included in other radiative transfer models (Gastellu-Etchegorry et al., 1996; Huemmrich, 2000) that may be used instead of SAIL to generate another database.

The database computation might be improved in some particular aspects: more types of soils, understory, and variation of other parameters like leaf angle or sun and view angles. One other way to proceed would be to create more targeted database using *a priori* knowledge of the measured canopy, and therefore limit the range of parameter variation.

Most types of indices were originally designed to be insensitive to specific changes of the reflectance spectrum. For instance, the D-type (simple difference between two wavelengths) is insensitive to additive changes of the reflectance, and the simple ratio (SR) and normalized difference (ND) types are insensitive to proportional effects. mND and mSR types of indices are insensitive to both additive and proportional effects. Our results show that taking into account the additive effects improves the efficiency of the index, since D-type indices give better results than simple R-type indices. Taking into account the proportional changes improves the results even more (SR compared to R-types) for all characteristics except LAI.

This is due to the fact that most of the leaf or canopy characteristics influence the spectra more in a proportional way than in an additive way. mSR and mND types in particular are insensitive to constant and proportional changes of reflectance, but our results show that they do not perform any better than ND indices, mostly because the inclusion of a supplementary wavelength increases the sensitivity to noise in the reflectance spectra and subsequent scattering.

Another advantage of the method is that it gives confidence in the generic character of the indices that were found at the leaf scale. Indeed, PROSPECT model was built to be as generic as possible, and was shown to be applicable to very different species, and even to needles (Zarco-Tejada et al., 2004a). One can say that changing the input parameters of PROSPECT or changing the species is the same thing. This generic character has been tested on the leaf reflectance database that has 49 different species.

At the canopy scale, things are very different because PROSAIL model cannot represent every possible forest. It represents a homogeneous closed canopy, without leaves or tree clumping, with particular soils and other characteristics (specified in the methods section for this study).

The methodology employed in this study, which uses a simulated reflectance database, has the major advantage of avoiding problems of covariance that often occur on measurement based studies. Indeed, when a measurement database is created at leaf or canopy level, some of the measured characteristics may have significant covariance. As a consequence, an index calibrated for a particular biophysical characteristic could in reality be linked to another characteristic. For instance, if measurements are conducted seasonally at different dates of growing season, there is a correlation between LAI and LMA. This decreases the generic application of such empirically-based indices. Using models avoids such problems because we can build simulated databases with independent variation of each characteristic. This gives strength and confidence to the indices we found.

Going further, we can say that the indices found for the simulation databases are exclusive, i.e. if an index is highly correlated to a particular characteristic, it cannot be correlated to another. This simple deduction enables a gross illustration as a matrix. Fig. 13 shows the areas of the ND index that give the best RMSE for the estimation of each input parameter of the PROSPECT and PROSAIL models. The area in grey does not correlate well to any input parameters (i.e. is sensitive to more than one parameter). Notably,

the up-scaling from leaf to canopy level modifies the arrangement of the efficient ND regions. The CHL and LMA regions basically remain the same between both scales, which means that no other physical variables added in the change of scale influence the indices in these regions. In contrast, the N_{struct} regions change substantially between the scales because of LAI, which has an effect that is very similar to N_{struct}. Most of the time N_{struct} regions are replaced by C_w regions. Note that at canopy scale the LAI regions are underestimated since the representation is based on an ND index instead of a D index, which is better for LAI determinations.

A closer look at the obtained indices reveals interesting features. A common characteristic is that one of the two reflectances is correlated to the studied parameter (ρ_{710} nm for CHL, ρ_{2260} nm for LMA, ρ_{970} nm for LAI, and ρ_{2160} nm for B_{leaf}), whereas the other is not correlated. For the CHL the most sensitive wavelength is located in the red-edge region near the red peak chlorophyll absorption because of less saturation for high chlorophyll content. Concerning LMA, the wavelength around 2260 nm corresponds to the better compromise between low water specific absorption and high dry matter specific absorption (according to PROSPECT). Notably, the other wavelength, 1490 nm, has almost exactly the same water specific absorption coefficient as the 2260 nm wavelengths (23.2 cm^{-1} and 22.0 cm^{-1}, respectively). Since reflectance is exponentially correlated to the sum of absorption of the different absorbing components, the use of ratio based indices (such as ND and SR) with two wavelengths having the same specific absorption coefficient (here 1490 and 2260 nm for water) cancel out the effect of this component. This explains why the ND_{LMA} index is strongly related to LMA and almost insensitive to leaf water content, even if the selected wavelengths are in the SWIR region. Concerning LAI, the selected sensitive wavelength corresponds to a region of high scattering effects inside the canopy (970 nm), whereas the other one (1725 nm) corresponds to a region of high water absorption and low reflectance value. B_{leaf} wavelengths (1540 nm and 2160 nm) are more influenced by LMA wavelengths than LAI wavelengths.

The wavelengths we found are generally consistent with the findings of Thenkabail et al. (2004), who recommended 22 bands for multi-spectral remote sensing of vegetation. Our CHL ND index (710 nm and 925 nm) combines Thenkabail's bands 5 (705 nm, Red-Edge 1) and 8 (915–935 nm, NIR2). Our LMA ND index (1490 nm and 2260 nm) is close to Thenkabail's bands 15 (1445 nm, EMIR1, sensitive to plant moisture) and 20 (2235 nm, FMIR3, sensitive to lignin, biomass and starch). Our LAI D index (970 nm and 1725 nm) is close to Thenkabail's bands 9 (985 nm, MSNIR, sensitive to plant moisture) and 17 (1725 nm, EMIR4, sensitive to biomass, cellulose and lignin). Our leaf biomass ND index (1540 nm and 2160 nm), however, is not close to any of Thenkabail's bands.

6. Conclusion

To obtain generic and widely applicable canopy biophysical indices, the methodology chosen was to find the best possible indices without a priori knowledge of wavelengths, by testing every possible combination on a synthetic database. At the canopy level, results from very different experimental datasets were found to be consistent and well aligned for each retrieved quantity (CHL, LMA, LAI and B_{leaf}). The results are strengthened by the experimental aspect of this work based on two different sites, and two different satellite images, with different local (soil types, fertility, age of the forest, species mixture and sampling date) and remote-sensed image conditions (atmospheric conditions, angles of view and sun). The obtained indices were found to apply successfully to both sites (between Fougères and Fontainebleau) and sensors (Hyperion or in situ Fieldspec). This gives more confidence in carrying on the development of a regression approach based on synthetic data and avoiding in situ measurement calibration.

The best indices at canopy scale are for leaf chlorophyll content: $ND_{Chl} = \frac{\rho_{925}-\rho_{710}}{\rho_{925}+\rho_{710}}$, for leaf mass per area: $ND_{LMA} = \frac{\rho_{1490}-\rho_{2260}}{\rho_{1490}+\rho_{2260}}$, for leaf area index: $D_{LAI}=\rho_{970}-\rho_{1725}$, and for canopy leaf biomass: $ND_{B_{leaf}} = \frac{\rho_{1540}-\rho_{2160}}{\rho_{1540}+\rho_{2160}}$. They showed good results with an RMSE of 8.1 μg cm^{-2} for CHL, 9.1 g m^{-2} for LMA, 1.7 m^2 m^{-2} for LAI and 50.6 g m^{-2} for B_{leaf}. However, at the canopy scale, even though the wavelengths were accurately determined with the simulated database, the regression itself had to be calibrated with respect to measurements.

In this study, we used only narrow band indices, but our results suggest that for some indices larger bands could be used. This is the case for ND types, where there are large areas of low RMSE in the RMSE matrix. It is also possible to imagine indices combining spectral bands of different sizes. For instance, in the CHL index $ND_{710,925}$, a narrow band close to 710 nm and a larger band between 800 and 1000 nm could be used. The best signal-to-noise ratio in the near infra-red region can be achieved without reducing the ability to retrieve canopy variables.

The methodology and published indices should now be tested on other images, sites and canopies to see if the presented results are confirmed in terms of wavelength, regression relationships and accuracy.

Acknowledgements

We would like to thank the Office National des Forêts (ONF, the French National Office for Forestry) for making possible in situ LAI measurements and for providing us with the forest GIS database. This work was also supported by the GIP-Ecofor and ORE F-ORE-T. We would like to thank the anonymous reviewers for their valuable comments and constructive feedback.

Appendix A. Description of the multi-layer PROSAIL model parameterization

Gradients of LMA and CHL were measured on *Fagus sylvatica* and *Quercus petraea* at the Hesse forest and are presented in Fig. A1. The LMA exponentially decreases inside the canopy, and is a function of the cumulative LAI.

$$LMA_i = LMA_0 \times \exp\left(-k_{LMA}\sum_{j=0}^{i} LAI_j\right)$$

where i stands for the layer number from the top, LMA_i and LAI_i are the LMA and LAI of the jth layer, and k_{LMA} is a constant. k_{LMA} (0.18) was obtained at the Hesse site and is very close to other values given in the literature (Davi, 2004), which gives confidence in its generality for broadleaved deciduous trees. The values of LMA_0 and the LAI profile are the input parameters of the multi-layer PROSAIL.

Chlorophyll per unit of leaf surface is approximately constant inside the canopy (Fig. A1). This is not always true: some stands show up to a 20% a decrease from top to bottom, while others show an increase. Tests have shown, however, that including a slight vertical profile of CHL does not significantly change PROSAIL output.

The structural parameter of PROSPECT is also considered constant inside the canopy. There is experimental evidence that the N_{struc} (introduced in 2.1) parameters are correlated to the LMA of the leaf, and therefore should decrease from the top to the bottom of the canopy. However this correlation is weak, so it is not possible to directly obtain it from LMA.

The leaf angles are generally more erectophile at the top layers and planophile at the bottom layers. For example, the mean angle of a *Nothofagus solandri* canopy changes from 40 to 20° from top to bottom (Hollinger, 1989). The vertical distribution of the leaves is due to the radiation gradient inside the canopy. For the simulations, we have considered the leaf angles to be constant from top to bottom, mainly because there are very few data to calibrate an appropriate model of vertical leaf angle distribution.

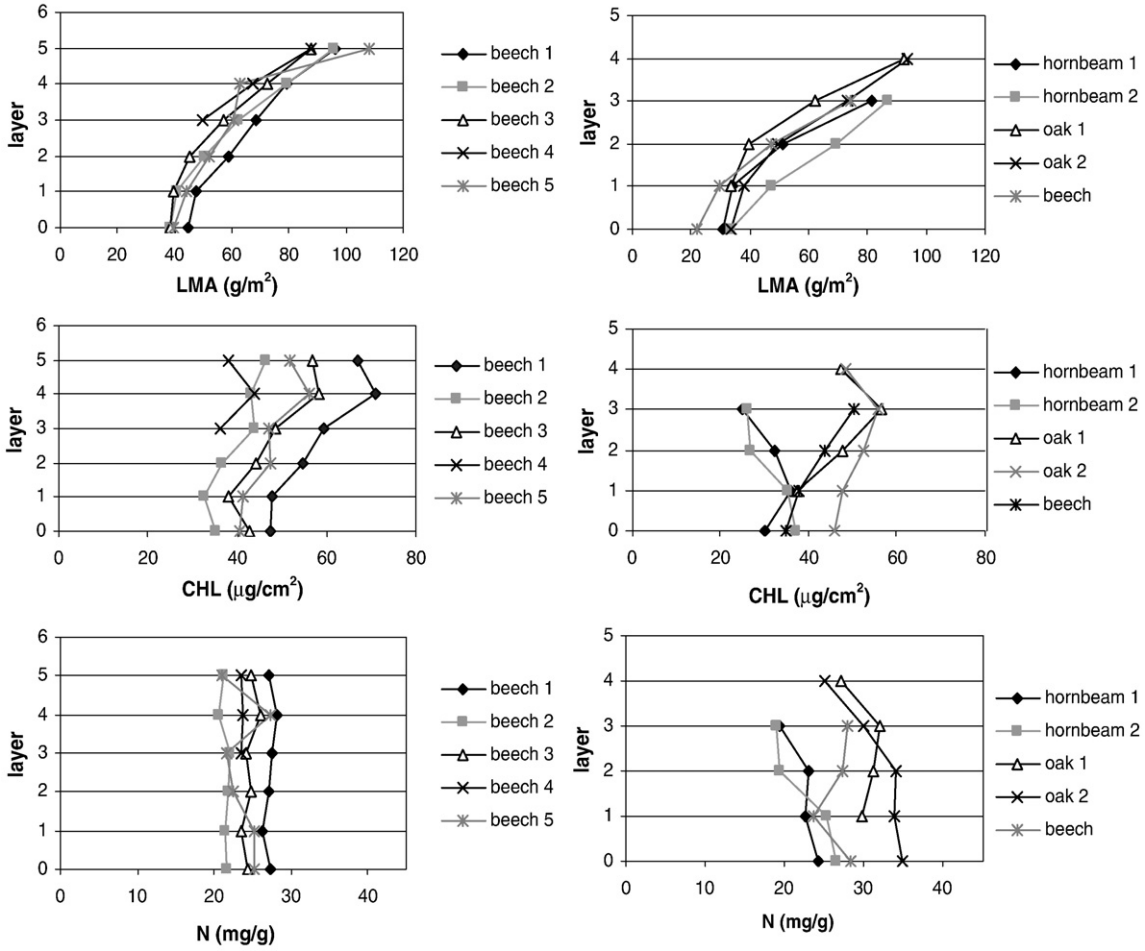

Fig. A1. Vertical profile of LMA (g m^{-2}), CHL (µg cm^{-2}) and N (mg g^{-1}) measured at Hesse site on two different stands (HESSE1 left and HESSE2 right). Layer thickness is about 1 m. Measurements have been made from top (sun leaves) to bottom. HESSE1 and HESSE2 are about 17 .5 m and 5 m height, respectively.

The soil reflectance is obtained from measurements of two soils: a brown dry soil and a wet soil (Broge and Leblanc, 2001). The soil reflectance is calculated as a weighted mean of these two soil reflectances, with the parameter p_{soil} equal to 0 for wet soil and 1 for dry soil. This very simple model was able to capture the main soil features by a direct fit. Three soils were used in the database corresponding to the two extremes ($p_{soil}=0$ and $p_{soil}=1$) and an average soil ($p_{soil}=0.5$).

Appendix B. Small trees canopy: LAI, LMA, CHL and canopy reflectance measurements

B.1. Seasonal monitoring

A temporal series of measurements was conducted during the 2002 growing season from leaf budburst to yellowing at two different places in the small canopy. Reflectance measurements were made at one meter height, with the sun close to its zenith (local noon) and clear sky (see reflectance measurement protocol at chapter 2.2.2). In parallel, chlorophyll was measured on sunleaves with a SPAD (Minolta Camera, Osaka, Japan) chlorophyll meter (average of about 100 measurements on 20 leaves). SPAD values were converted to chlorophyll values using a precisely calibrated relationship ($CHL = -0.00023453 * SPAD^3 + 0.0626 * SPAD^2 - 1.1372401 * SPAD + 10.33$). SPAD measurements were also made on the top, middle and bottom layers to ensure that it did not change vertically. LMA was measured by taking 10 sunleaves just around the measurement footprint to avoid changing the canopy structure between two measurements. Leaf surfaces were measured, oven dried and weighted to obtain their LMA. The LMA vertical decrease was also measured. Concerning the LAI, because destructive measurements were not possible, we directly measured all leaf surfaces using a relationship $Surface = 0.71 * L * w$ (L=length, w=width). The leaves were measured and counted above a given surface, chosen approximately to be the field of view of the spectroradiometer. LAI was calculated as the ratio of the total leaf area to the ground surface. This configuration of measurements allowed reflectance measurements with highly variable LAI, LMA and CHL, with most of the changes, however, co-occurring. The measurements are reported in Table 4.

B.2. Spatial measurements

Another experiment was done during one clear day in June 2003. When the sun was close to its zenith (local noon), four different measurements were done in four locations of the small canopy. The protocol for LAI, LMA, and CHL determination was the same as above.

B.3. Potted tree spacing

The third protocol was devised to artificially change the LAI using potted trees that were planted concurrently with the small canopy. These black pots were placed on a surface covered with the same mould as the small canopy. The first reflectance measurement was made with the four pots that were stuck together, as the leaves of each tree were entangled. The pots were then moved away from each other,

and new measurements were made. This was repeated nine times, the last measurement being made without any leaves in the field of view. All measurements were done in a one-hour time frame on the same day in June 2003 with a clear sky and the sun at local noon. We assume that small sun angle changes occurring during this period did not strongly affect the reflectance signal with a nadir observation. Between two consecutive measurements, tree density decreased, there were fewer leaves present in the field of view, and LAI decreased. CHL and LMA, however, did not change. LAI, CHL and LMA measurements were made with the same methodology as that used for the small canopy, except that leaves could be sampled at the end of the experiment on leaves that were inside the field of view.

B.4. Defoliation

Finally, a total defoliation of a part of the small canopy was performed during one week in June 2004. Reflectance of this surface was measured at the same solar time (local noon), with the spectroradiometer at 1.5 m, because trees were of one meter height in 2004. Between two reflectance measurements, 240 leaves were randomly taken from the canopy within a delimited zone that included the surface seen by the sensor. To make sure that leaves were randomly selected, the vertical dimension was divided into top, middle and bottom layers, and one third of the 240 leaves were taken from each layer. Twenty-six reflectance measurements were made before the canopy was totally defoliated. All leaves were kept cold before their surface measurement with a planimeter for the LAI calculation. The initial LAI was calculated when all the leaves were taken and measured, and intermediate LAI was calculated by difference. The leaves were oven dried and weighted to obtain their mean LMA. CHL was obtained from SPAD measurements.

Appendix C. Fontainebleau and Fougères forests: LAI, LMA and CHL measurements

The same measurement protocols were used in Fontainebleau and Fougères. Five to 15 representative trees were selected within each stand: five trees in Fontainebleau stands or 10 in case of mixed stands (five trees per species), 10 trees in Hesse or 15 in case of mixed stands (10 beech trees and five oak trees). For each selected tree, one branch of the upper canopy exposed to sunlight was shot. 3*10 leaves were randomly selected and placed into three different bags, with one of them chosen for chlorophyll content measurements. For each of the ten leaves of that bag, 6 to 15 SPAD measurements spaced by 1 to 2 cm were made all over the leaf. The average SPAD value was calculated for each leaf. The average SPAD value per leaf was then used to obtain leaf chlorophyll (in μg cm^{-2}) with the same equation used in the small canopy method (Appendix B). The average of the 10 chlorophyll estimations gives the tree chlorophyll estimate and the average of tree estimates gives the stand CHL estimate.

The three bags per tree, each containing ten leaves, were used for LMA estimation. The cumulative surface of the ten leaves was measured with an area meter (LI-3000A Area Meters, LI-COR Inc., Nebraska), and then leaves were oven-dried for two days at 60–65 °C before being weighted. The LMA is the ratio of the leaf surface to dry weight (g m^{-2}). The three values per tree were averaged to get the tree LMA estimate, and the average of tree estimates is the stand LMA estimate.

The LAI-2000 was used for ground LAI measurements. A detailed description of this instrument is given by Cutini et al. (1998). Calculations were carried out using three rings, which give an approximate value for the integration surface covered by the LAI-2000 of 300 m^2, depending on tree height. A detailed description and analysis of the LAI measurement method is given by Dufrêne and Bréda (1995), Le Dantec et al. (2000), and Soudani et al. (2006). For each stand, and according to its size, 40 to 150 LAI-2000 measurements were taken at intervals of 8±2 m on several transects. For the Fougères site, the LAI measurements were made in 28 of the 33 stands.

Appendix D. Hyperion image processing

Bad pixel removal: Bad pixels are already flagged in the L1R during the USGS processing. However, we performed an additional search for bad pixels with the Han et al. (2002) methodology. Negative pixel values were replaced by null values. Pixels in a given column for which values were inferior to their left and right adjacent pixels were marked. If more than half of the pixels of a column were marked, and if there were at least 15 contiguous marked pixels in a column, then the column was corrected, i.e. replaced by the mean of the adjacent columns.

Destriping: For some bands, there were stripes, generally at the left and right part of the image. The destriping methodology used is a new and efficient one, that is improved from the "global method" described by Datt et al. (2003). The global method calculates a gain g_i and an offset o_i for the ith column of the image for a given band, with the following equations:

$$g_i = \frac{s}{s_i}$$
$$o_i = m - g_i \times m_i$$

where m and s are the mean and standard deviation of the entire image (for the considered band) and m_i and s_i are those of the considered column.

Finally, the pixel x_{ij} (ith column, jth row) is corrected with:

$$x_{ijcorrected} = x_{ij} \times g_i + o_i.$$

This means that the mean and standard deviation of each column after correction are equal to those of the entire image. As noted by Datt et al. (2003), this leads to high incoherencies in images taken for landscapes that are spatially heterogeneous in reflectance like Fontainebleau and Fougères, and that are not equally distributed in the horizontal axis. For instance, a large sandpit (high reflectance) is located in the south-east of the Fontainebleau forest, resulting in s_i and m_i that are very different from other columns.

The new methodology is based on a modified "local method" that uses non-striped bands spectrally close to the ones subject to correction. A linear equation is obtained by comparing the pixel values of these two bands (only pixels of the column 88 to 168 are used because they have fewer stripes). The non-striped image is then transformed to a new image I with this equation. The equations are the same as for the global method, except that m and s values are replaced by m_{Ii} and s_{Ii}, the mean and standard deviation of the transformed image I for the column i. Fig. A2 shows the mean and standard deviation of the column of band 8 before and after destriping. The column standard deviation does not change much after image destriping.

Smile effect: This step aims to correct the signal for cross-track spectral errors (smile/frown). Hyperion's two dimensional detector arrays show a frown effect of 2.6 nm to 3.6 nm and .40 nm to .97 nm in the VNIR and SWIR, respectively. A linear interpolation resampling scheme has been applied to the data using the spectral calibration file provided with the level 1R data to remove this effect. The smile effect may have changed with time since launch (Khurshid et al., 2006), but this change may only have a small effect on the result obtained in this study.

Atmospheric corrections: This step aims to correct the signal for the atmospheric absorption and scattering mainly due to water vapor and aerosols. This was done with the FLAASH (Fast Line-of-sight Atmospheric Analysis of Spectral Hypercubes) software incorporated in ENVI based on the MODTRAN (MODerate resolution atmospheric

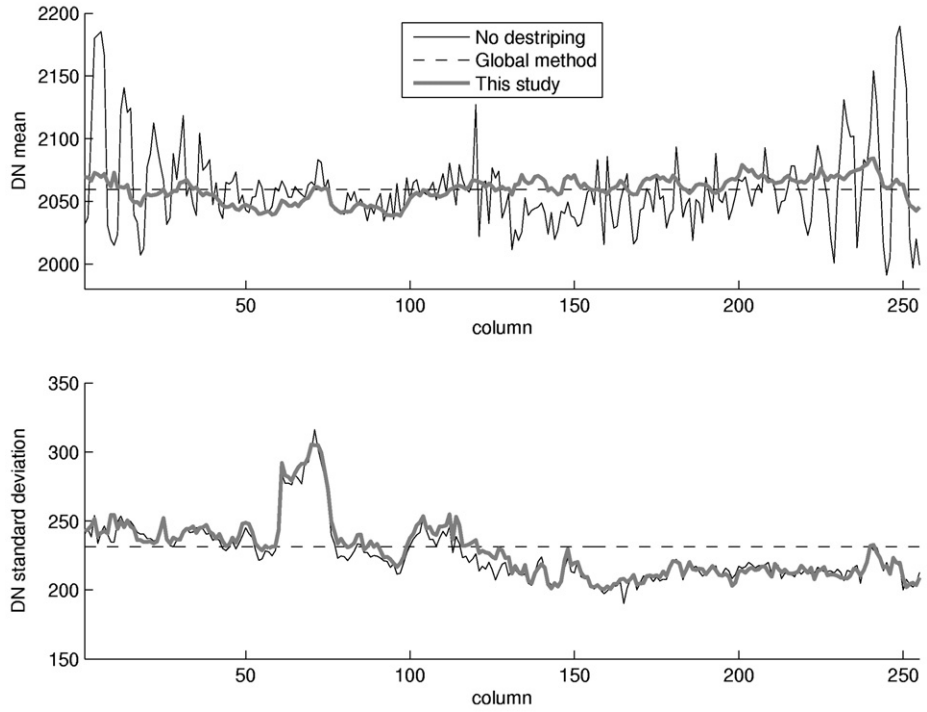

Fig. A2. Mean and standard deviation DN for band 8 (per column) of Fontainebleau Hyperion image for original image, and destriped image with the global method or the method used for this study.

TRANsmission) model. For the Fontainebleau forest, the water vapor content and the optical depth of aerosols were prescribed at their values measured on the day of acquisition with a Cimel (CE 318N, Cimel Electronique, France) sun photometer placed in the centre of the forest, and part of the AERONET (AErosol RObotic NETwork) global network. For the Fougères forest, the water and aerosol retrieval of FLAASH were used. These options have shown successful results when applied in Fontainebleau. The aerosol model for Fontainebleau is urban due to the proximity of Paris, whereas for Fougères the aerosol model is rural.

Georeferencing and rectification: This was done using about 20 ground control points from 1:25,000 maps and GPS ground measurements at distinct points inside or around the forest. The landscape is mainly flat in Fontainebleau and Fougères, so that rectification with a second order polynomial is sufficient to reduce error below 15 m.

References

Anderson, M. C., Neale, C. M. U., Li, F., Norman, J. M., Kustas, W. P., Jayanthi, H., et al. (2004). Upscaling ground observations of vegetation water content, canopy height, and leaf area index during SMEX02 using aircraft and Landsat imagery. *Remote sensing of environment*, *92*, 447–464.

Andrieu, B., Baret, F., Jacquemoud, S., Malthus, T., & Steven, M. (1997). Evaluation of an improved version of SAIL model for simulating bidirectional reflectance of sugar beet canopies. *Remote sensing of environment*, *60*, 247–257.

Atzberger, C. (2004). Object-based retrieval of biophysical canopy variables using artificial neural nets and radiative transfer models. *Remote sensing of environment*, *93*, 53–67.

Bacour, C., Baret, F., Beal, D., Weiss, M., & Pavageau, K. (2006). Neural network estimation of LAI, fAPAR, fCover and LAIxC(ab), from top of canopy MERIS reflectance data: principles and validation. *Remote sensing of environment*, *105*, 313–325.

Baret, F., Hagolle, O., Geiger, B., Bicheron, P., Miras, B., Huc, M., et al. (2007). LAI, fAPAR and fCover CYCLOPES global products derived from VEGETATION: Part 1: Principles of the algorithm. *Remote sensing of environment*, *110*, 275–286.

Birky, A. K. (2001). NDVI and a simple model of deciduous forest seasonal dynamics. *Ecological Modelling*, *143*, 43–58.

Blackburn, G. A. (2007). Hyperspectral remote sensing of plant pigments. *Journal of Experimental Botany*, *58*, 855–867.

Broge, N. H., & Leblanc, E. (2001). Comparing prediction power and stability of broadband and hyperspectral vegetation indices for estimation of green leaf area index and canopy chlorophyll density. *Remote sensing of environment*, *76*, 156–172.

Broge, N. H., & Mortensen, J. V. (2002). Deriving green crop area index and canopy chlorophyll density of winter wheat from spectral reflectance data. *Remote sensing of environment*, *81*, 45–57.

Campbell, G. S. (1986). Extinction coefficients for radiation in plant canopies calculated using an ellipsoidal inclination angle distribution. *Agric. For. Meteorol.*, *36*, 317–321.

Combal, B., Baret, F., Weiss, M., Trubuil, A., Mace, D., Pragnere, A., et al. (2003). Retrieval of canopy biophysical variables from bidirectional reflectance: using prior information to solve the ill-posed inverse problem. *Remote sensing of environment*, *84*, 1–15.

Coops, N. C., Smith, M. L., Martin, M. E., & Ollinger, S. V. (2003). Prediction of eucalypt foliage nitrogen content from satellite-derived hyperspectral data. *Ieee Transactions on Geoscience and Remote Sensing*, *41*, 1338–1346.

Cutini, A., Matteucci, G., & Mugnozza, G. S. (1998). Estimation of leaf area index with the Li-Cor LAI 2000 in deciduous forests. *Forest Ecology and Management*, *105*, 55–65.

Datt, B., McVicar, T. R., Van Niel, T. G., Jupp, D. L. B., & Pearlman, J. S. (2003). Preprocessing EO-1 Hyperion hyperspectral data to support the application of agricultural indexes. *Ieee Transactions on Geoscience and Remote Sensing*, *41*, 1246–1259.

Davi, H. (2004). Développement d'un modèle forestier générique simulant les flux et les stocks de carbone et d'eau dans le cadre des changements climatiques (Thèse de doctorat - PhD Thesis) (p. 194). Orsay: Université Paris XI.

Davi, H., Bouriaud, O., Dufrene, E., Soudani, K., Pontailler, J. Y., le Maire, G., et al. (2006). Effect of aggregating spatial parameters on modelling forest carbon and water fluxes. *Agricultural and Forest Meteorology*, *139*, 269–287.

Dufrêne, E., & Bréda, N. (1995). Estimation of deciduous forest leaf area index using direct and indirect methods. *Oecologia*, 156–162.

Dufrêne, E., Davi, H., François, C., le Maire, G., Le Dantec, V., & Granier, A. (2005). Modelling carbon and water cycles in a beech forest: part I: model description and uncertainty analysis on modelled NEE. *Ecological Modelling*, *185*, 407–436.

Fassnacht, K. S., Gower, S. T., MacKenzie, M. D., Nordheim, E. V., & Lillesand, T. M. (1997). Estimating the leaf area index of North Central Wisconsin forests using the landsat thematic mapper. *Remote sensing of environment*, *61*, 229–245.

Feret, J. B., François, C., Asner, G. P., Gitelson, A. A., Martin, R. E., Bidel, L., et al. (2008). PROSPECT-4 and 5: Advances in the Leaf Optical Properties Model Separating Photosynthetic Pigments. *Remote Sensing of Environment*, *112*, 3030–3043.

Filella, I., Serrano, L., Serra, J., & Peñuelas, J. (1995). Evaluating wheat nitrogen status with canopy reflectance indices and discriminent analysis. *Crop Science*, *35*, 1400–1405.

Gastellu-Etchegorry, J. P., Demarez, V., Pinel, V., & Zagolski, F. (1996). Modeling radiative transfer in heterogeneous 3-d vegetation canopies. *Remote sensing of environment*, *76*, 1–15.

Gitelson, A. A., Gritz, Y., & Merzlyak, M. N. (2003). Relationships between leaf chlorophyll content and spectral reflectance and algorithms for non-destructive chlorophyll assessment in higher plant leaves. *J Plant Physiol*, *160*, 271–282.

Goel, N. S., & Thomson, R. L. (1984). Inversion of vegetation canopy reflectance models for estimating agronomic variables. *IV. Total inversion of the SAIL model. Remote sensing of environment*, *15*, 237–251.

Han, T., Goodenough, D. G., Dyk, A., & Love, J. (2002). Detection and correction of abnormal pixels in hyperion images, geoscience and remote sensing symposium, 2002. *IGARSS '02* (pp. 1327–1330). Toronto, Ontario, Canada: IEEE.

Hansen, P. M., & Schjoerring, J. K. (2003). Reflectance measurement of canopy biomass and nitrogen status in wheat crops using normalized difference vegetation indices and partial least squares regression. *Remote sensing of environment*, *86*, 542–553.

Hollinger, D. Y. (1989). Canopy organization and foliage photosynthetic capacity in a broad-leaved evergreen montane forest. *Functional Ecology*, *3*, 53–62.

Huemmrich, K. F. (2000). *BOREAS TE-18 GeoSail Canopy Reflectance Model.*

Jacquemoud, S., & Baret, F. (1990). PROSPECT: a model of leaf optical properties spectra. *Remote Sens. Environ.*, *34*, 75–91.

Jacquemoud, S., Ustin, S. L., Verdebout, J., Schmuck, G., Andreoli, G., & Hosgood, B. (1996). Estimating leaf biochemistry using the PROSPECT leaf optical properties model. *Remote sensing of environment*, *56*, 194–202.

Khurshid, K. S., Staenz, K., Sun, L. X., Neville, R., White, H. P., Bannari, A., et al. (2006). Preprocessing of EO-1 hyperion data. *Canadian Journal of Remote Sensing*, *32*, 84–97.

Kimes, D. S., Knyazikhin, Y., Privette, J. L., Abuelgasim, A. A., & Gao, F. (2000). Inversion methods for physically-based models. *Remote Sensing Reviews*, *18*, 381–439.

Knyazikhin, Y., Martonchik, J. V., Diner, D. J., Myneni, R. B., Verstraete, M., Pinty, B., et al. (1998). Estimation of vegetation canopy leaf area index and fraction of absorbed photosynthetically active radiation from atmosphere-corrected MISR data. *Journal of Geophysical Research-Atmospheres*, *103*, 32239–32256.

Kubelka, P., & Munk, F. (1931). Ein Betrag zur Optik der Farbanstriche. *Ann. Tech. Phys.*, *11*, 593–601.

Landsberg, J. (2003). Modelling forest ecosystems: state of the art, challenges, and future directions. *Canadian Journal of Forest Research*, *33*, 385–397.

Le Dantec, V., Dufrene, E., & Saugier, B. (2000). Interannual and spatial variation in maximum leaf area index of temperate deciduous stands. *Forest Ecology and Management*, *134*, 71–81.

le Maire, G., Davi, H., François, C., Soudani, K., Le Dantec, V., & Dufrêne, E. (2005). Modelling annual production and carbon fluxes of a large managed temperate forest using forest inventories, satellite data and field measurements. *Tree Physiology*, *25*, 859–872.

le Maire, G., Francois, C., & Dufrene, E. (2004). Towards universal broad leaf chlorophyll indices using PROSPECT simulated database and hyperspectral reflectance measurements. *Remote sensing of environment*, *89*, 1–28.

le Maire, G., Francois, C., Soudani, K., Davi, H., Le Dantec, V., Saugier, B., et al. (2006). Forest leaf area index determination: a multiyear satellite-independent method based on within-stand normalized difference vegetation index spatial variability. *Journal of Geophysical Research-Biogeosciences*, *111*, G02027. doi:10.1029/2005JG000122

Major, D. J., Schaalje, G. B., Wiegand, C., & Blad, B. L. (1992). Accuracy and sensitivity analyses of SAIL model-predicted reflectance of maize. *Remote sensing of environment*, *41*, 61–70.

Makela, A., Landsberg, J., Ek, A. R., Burk, T. E., Ter-Mikaelian, M., Agren, G. I., et al. (2000). Process-based models for forest ecosystem management: current state of the art and challenges for practical implementation. *Tree Physiology*, *20*, 289–298.

Moran, J. A., Mitchell, A. K., Goodmanson, G., & Stockburger, K. A. (2000). Differentiation among effects of nitrogen fertilization treatments on conifer seedlings by foliar reflectance: a comparison of methods. *Tree Physiology*, *20*, 1113–1120.

Qi, J., Kerr, Y. H., Moran, M. S., Weltz, M., Huete, A. R., Sorooshian, S., et al. (2000). Leaf area index estimates using remotely sensed data and BRDF models in a semiarid region. *Remote sensing of environment*, *73*, 18–30.

Smith, M. L., Martin, M. E., Plourde, L., & Ollinger, S. V. (2003). Analysis of hyperspectral data for estimation of temperate forest canopy nitrogen concentration: comparison between an airborne (AVIRIS) and a spaceborne (Hyperion) sensor. *Ieee Transactions on Geoscience and Remote Sensing*, *41*, 1332–1337.

Soudani, K., Francois, C., le Maire, G., Le Dantec, V., & Dufrene, E. (2006). Comparative analysis of IKONOS, SPOT, and ETM+ data for leaf area index estimation in temperate coniferous and deciduous forest stands. *Remote sensing of environment*, *102*, 161–175.

Suits, G. H. (1972). The calculation of the directional reflectance of a vegetative canopy. *Remote Sensing of the Environment*, *2*, 117–125.

Thenkabail, P. S., Enclona, E. A., Ashton, M. S., & Van der Meer, B. (2004). Accuracy assessments of hyperspectral waveband performance for vegetation analysis applications. *Remote sensing of environment*, *91*, 354–376.

Verhoef, W. (1984). Light scattering by leaf layers with application to canopy reflectance modeling: The SAIL model. *Remote sensing of environment*, *16*, 125–141.

Wang, Q., Adiku, S., Tenhunen, J., & Granier, A. (2005). On the relationship of NDVI with leaf area index in a deciduous forest site. *Remote sensing of environment*, *94*, 244–255.

Weiss, M., & Baret, F. (1999). Evaluation of canopy biophysical variable retrieval performances from the accumulation of large swath satellite data. *Remote sensing of environment*, *70*, 293–306.

Weiss, M., Troufleau, D., Baret, F., Chauki, H., Prevot, L., Olioso, A., et al. (2001). Coupling canopy functioning and radiative transfer models for remote sensing data assimilation. *Agricultural and Forest Meteorology*, *108*, 113–128.

Yoder, B. J., & Pettigrew-Crosby, R. E. (1995). Predicting nitrogen and chlorophyll content and concentrations from reflectance spectra (400–2500 nm) at leaf and canopy scales. *Remote sensing of environment*, *53*, 199–211.

Zarco-Tejada, P. J., Miller, J. R., Harron, J., Hu, B., Noland, T. L., Goel, N., et al. (2004). Needle chlorophyll content estimation through model inversion using hyperspectral data from boreal conifer forest canopies. *Remote sensing of environment*, *89*, 189–199.

Zarco-Tejada, P. J., Miller, J. R., Morales, A., Berjon, A., & Aguera, J. (2004). Hyperspectral indices and model simulation for chlorophyll estimation in open-canopy tree crops. *Remote sensing of environment*, *90*, 463–476.

Zarco-Tejada, P. J., Miller, J. R., Noland, T. L., Mohammed, G. H., & Sampson, P. (2001). Scaling up and model inversion methods with narrow-band optical indices for chlorophyll content estimation in closed forest canopies with hyperspectral data. *IEEE Transactions on Geoscience and Remote Sensing*, *39*, 1491–1501.

Zhao, D. L., Reddy, K. R., Kakani, V. G., Read, J. J., & Koti, S. (2005). Selection of optimum reflectance ratios for estimating leaf nitrogen and chlorophyll concentrations of field-grown cotton. *Agronomy Journal*, *97*, 89–98.